

# Multi-method absolute paleointensity determinations on a Pliocene multiple-polarity record from the Lesser Caucasus

Elisa María Sánchez-Moreno<sup>1</sup>, Manuel Calvo-Rathert<sup>1</sup>, Avto Goguitchaichvili<sup>2</sup>, George T. Vashakedze<sup>3</sup>, Pierre C Camps<sup>4</sup>, Juan Morales<sup>5</sup>, Néstor Vegas<sup>6</sup>, and Vladimir A. Lebedev<sup>7</sup>

<sup>1</sup>Universidad de Burgos

<sup>2</sup>Instituto de Geofísica, U.N.A. M.

<sup>3</sup>Alexandre Janelidze Institute of Geology - Ivane Javakhishvili Tbilisi State University

<sup>4</sup>CNRS & Univ. Montpellier

<sup>5</sup>Unknown

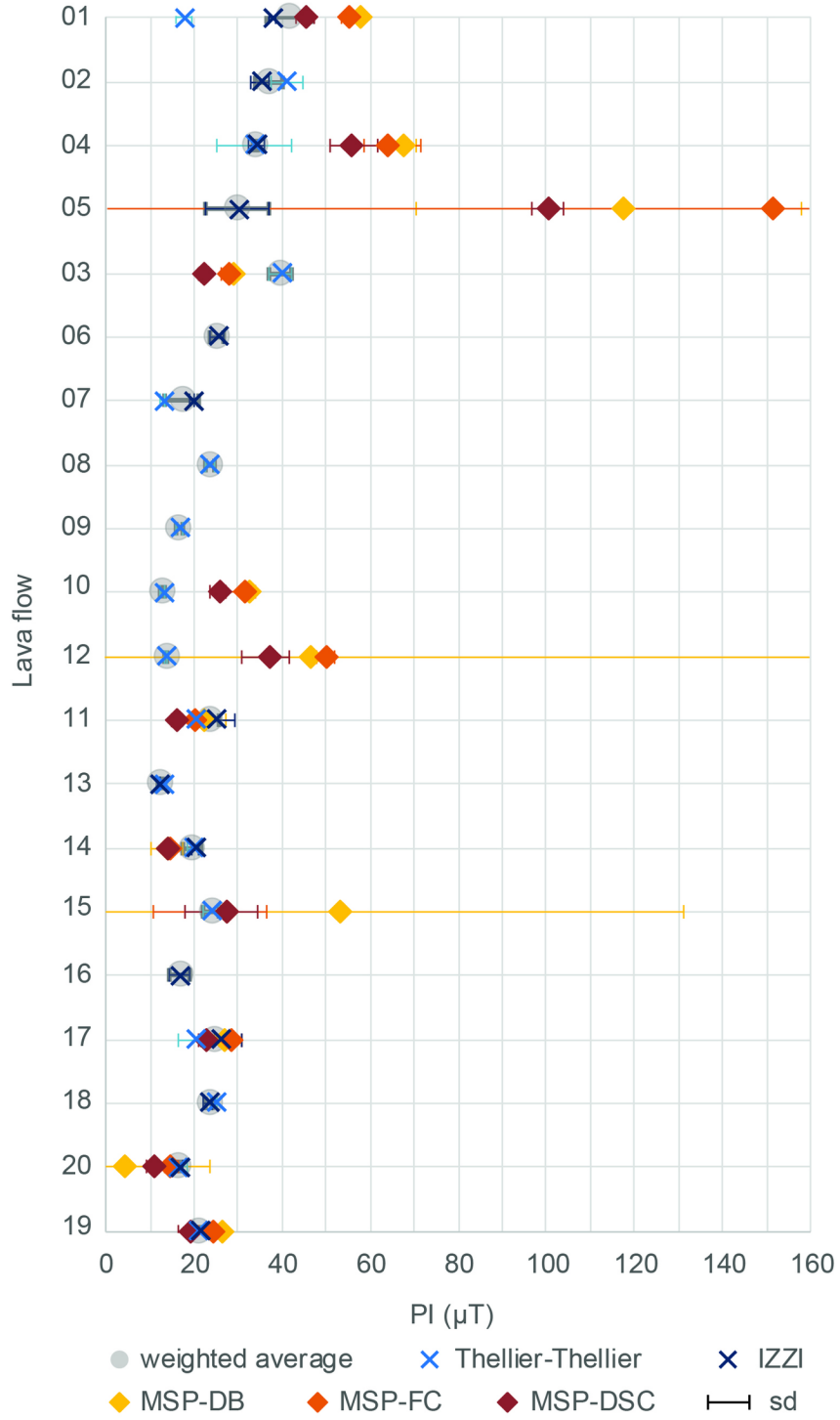
<sup>6</sup>Universidad del País Vasco (UPV/EHU)

<sup>7</sup>IGEM - RAS

November 24, 2022

## Abstract

We report high technical quality absolute paleointensity determinations from a Pliocene sequence of 20 consecutive lava flows sampled in South Georgia named Apnia, which record either the Gilbert-Gauss polarity reversal or a composite transition from chron C2Ar to subchron C2An-2n. Paleointensity determinations with the multispecimen (MSP) technique were performed on 12 samples with both the original method (MSP-DB) and the extended protocol with corrections (MSP-DSC). Six MSP-DB and eight MSP-DSC determinations passed the proposed quality criteria. MSP-DB yielded higher intensity values than MSP-DSC. In order to provide additional reliability to the results, we have carried out a consistency test by means of a multi-method approach. We have compared the MSP intensities with Thellier-type intensities obtained from the reinterpretation of determinations performed in previous study. The match of both types of paleointensity determinations gives the results an added reliability. Paleointensity results have been obtained in all 20 flows, 11 of which were supported on different methods. At the reverse polarity lower section, low-VADM values between  $2.1$  and  $4.2 \times 10$  Am were obtained. The single transitional flow displayed  $4.3 \times 10$  Am, and the normal polarity upper section showed higher values between  $5.1$  and  $7.1 \times 10$  Am. The lower section results might be a pre-reversal stage record and the upper section may reflect the intensity recovery after the complete reversal. Furthermore, the results comparison from both methods will allow the evaluation of the quality parameters proposed to MSP method, which are controversial given the novelty of the technique.



1 **Multi-method absolute paleointensity determinations on a Pliocene multiple-**  
2 **polarity record from the Lesser Caucasus**

3  
4 Elisa M. Sánchez-Moreno<sup>1,\*</sup>, Manuel Calvo-Rathert<sup>1,7</sup>, Avto Goguitchaichvili<sup>2</sup>, George T.  
5 Vashakidze<sup>3</sup>, Pierre Camps<sup>4</sup>, Juan Morales-Contreras<sup>2</sup>, Néstor Vegas-Tubía<sup>5</sup>, Vladimir A.  
6 Lebedev<sup>6</sup>

7  
8 <sup>1</sup>Departamento de Física, EPS Campus Rio Vena – Universidad de Burgos, Av.  
9 Cantabria, s/n, 09006 Burgos, Spain.

10 <sup>2</sup>Laboratorio Interinstitucional de Magnetismo Natural, Instituto de Geofísica Unidad  
11 Michoacán, UNAM – Campus Morelia, 58990 Morelia, México.

12 <sup>3</sup>Alexandre Janelidze Institute of Geology – Ivane Javakhishvili Tbilisi State University,  
13 1/9 M. Alexidze str., 0171 Tbilisi, Georgia.

14 <sup>4</sup>Géosciences Montpellier, Univ. Montpellier, CNRS, Montpellier, France.

15 <sup>5</sup>Departamento de Geodinámica, Universidad del País Vasco, E-48940 Leioa, Bizkaia,  
16 Spain.

17 <sup>6</sup>Institute of Geology of Ore Deposits, Petrography, Mineralogy and Geochemistry –  
18 Russian Academy of Sciences (IGEM RAS), Staromonetny per., 35, 119017 Moscow,  
19 Russia.

20 <sup>7</sup>Hawaii Institute of Geophysics and Planetology – University of Hawaii at Manoa, 1680  
21 East-West Rd., 96822 Honolulu, HI, United States.

22  
23 \*Corresponding author: [emsanchez@ubu.es](mailto:emsanchez@ubu.es)

24  
25 **Key points**

- 26  
27 - High reliable paleointensities supported by a multi-method consistency test  
28 - Paleointensity variability in a reverse, intermediate and normal-polarity record  
29 - Successful check of the corrections included in the MSP-DSC protocol

30  
31 **Abstract**

32  
33 We report high technical quality absolute paleointensity determinations from a  
34 Pliocene sequence of 20 consecutive lava flows sampled in South Georgia named  
35 Apnia, which record either the Gilbert-Gauss polarity reversal or a composite transition  
36 from chron C2Ar to subchron C2An-2n. Paleointensity determinations with the  
37 multispecimen (MSP) technique were performed on 12 samples with both the original  
38 method (MSP-DB) and the extended protocol with corrections (MSP-DSC). Six MSP-DB  
39 and eight MSP-DSC determinations passed the proposed quality criteria. MSP-DB  
40 yielded higher intensity values than MSP-DSC. In order to provide additional reliability  
41 to the results, we have carried out a consistency test by means of a multi-method  
42 approach. We have compared the MSP intensities with Thellier-type intensities  
43 obtained from the reinterpretation of determinations performed in previous study.  
44 The match of both types of paleointensity determinations gives the results an added

45 reliability. Paleointensity results have been obtained in all 20 flows, 11 of which were  
46 supported on different methods. At the reverse polarity lower section, low-VADM  
47 values between 2.1 and  $4.2 \times 10^{22} \text{ Am}^2$  were obtained. The single transitional flow  
48 displayed  $4.3 \times 10^{22} \text{ Am}^2$ , and the normal polarity upper section showed higher values  
49 between 5.1 and  $7.1 \times 10^{22} \text{ Am}^2$ . The lower section results might be a pre-reversal  
50 stage record and the upper section may reflect the intensity recovery after the  
51 complete reversal. Furthermore, the results comparison from both methods will allow  
52 the evaluation of the quality parameters proposed to MSP method, which are  
53 controversial given the novelty of the technique.

54

55 **Key words:** Thellier-Thellier protocol; IZZI protocol; Multispecimen protocols; multi-  
56 method paleointensities; high reliable paleointensities; Lesser Caucasus

57

## 58 1. Introduction

59

60 Both directional and intensity data are crucial to deeply understand the  
61 characteristics of the Earth's Magnetic Field during unstable periods such as reversals  
62 or excursions. While paleomagnetic directions can be obtained in a relatively direct  
63 way, the absolute paleointensity determination is more complex and time-consuming  
64 because the remanent magnetization is proportional, but not equal to the field  
65 intensity and there are many processes that can alter the constant of proportionality  
66 between both magnitudes. Paleointensity data are less than directional ones because  
67 they can only be obtained from materials where the primary magnetization is a  
68 thermo-remanent magnetization (TRM), like volcanic rocks. In addition, in  
69 paleointensity determinations magneto-chemical alteration of the remanence-carrying  
70 minerals should occur during the multiple heating and cooling steps. Furthermore, the  
71 laws of reciprocity, independence, and additivity of partial thermoremanent  
72 magnetization (pTRM) should be obeyed, which is only the case of the TRM recorded  
73 by single domain (SD) and small pseudo-single domain (PSD) grains (Thellier and  
74 Thellier, 1959; Dunlop, 2011 and references therein). Multidomain (MD) grains (s.l.)  
75 are characterized by different blocking and unblocking temperatures giving rise to so-  
76 called pTRM tails (Bol'shakov and Shcherbakova, 1979; Dunlop and Xu, 1994).

77

78 This work focuses on the joint analysis of new absolute paleointensity data  
79 obtained in the present study with the multispecimen (MSP) method (Biggin and  
80 Poidras 2006; Dekkers and Böhnell 2006; Fabian and Leonhardt 2007) and a collection  
81 of Thellier-type paleointensity determinations performed previously (Sánchez-Moreno,  
82 2018). This second group of determinations was carried out with the Thellier-Thellier  
83 (Thellier and Thellier, 1959) and the IZZI (Yu et al., 2004) methods and results were  
84 reinterpreted in this work applying a set of selection criteria commonly used in this  
85 type of studies (based on the classical ThellierTool criteria of Leonhardt et al. 2004).  
86 Paleointensity determination methods depend on how different energy equilibrium  
87 states related to temperature, applied field and demagnetising field are reached

88 during the experiments. Thus, the use of different methods based on different  
89 experimental procedures on samples of the same units, provides an additional strong  
90 reliability check with a multi-method consistency test (De Groot et al., 2013; Biggin and  
91 Paterson, 2014; Biggin et al., 2015; De Groot et al., 2015; Monster et al., 2015a; Calvo-  
92 Rathert et al., 2016; De Groot et al., 2016; Monster et al., 2018), which is one of the  
93 aims of the present study.

94

95 The MSP-DB is a relatively new paleointensity method supposed to be  
96 independent of magnetic domain structure because it presumably eliminates magnetic  
97 history effects. The protocol proposes to perform a single heating, trying to minimize  
98 the effect of magnetic history due to the presence of MD grains. Fabian and Leonhardt  
99 (2010), however, suggest that even so, this method systematically overestimates  
100 paleointensity on samples containing MD grains, and thus proposed some additional  
101 steps including pTRM normalization, domain-state correction, and an alteration test in  
102 a new protocol named multispecimen domain-state-correction (MSP-DSC). Michalk et  
103 al., (2010; 2008) and Calvo-Rathert et al., (2016) have also observed paleointensity  
104 overestimates with the MSP-DB method on lavas containing a significant MD fraction.  
105 Some other studies, however, point to similar values or underestimations with both  
106 protocols (Muxworthy and Taylor, 2011; De Groot et al., 2012; Tema et al., 2015, 2016;  
107 Calvo-Rathert et al., 2018). Therefore, another aim of the present study is to assess the  
108 quality and reliability of the MSP (mainly MSP-DSC) results by comparing them with  
109 Thellier-type determinations because the latter are based on a rigorous physical  
110 background.

111

112 MSP and Thellier-type paleointensity determinations analyzed in the present  
113 study have been carried out over the basaltic flow sequence of Apnia (Djavakheti  
114 Highland, Southern Georgia), which has been radiometrically dated by Lebedev et al.,  
115 (2008) yielding K-Ar ages ( $\pm 2\sigma$ ) between  $3.09 \pm 0.10$  to  $3.75 \pm 0.25$  Ma. The  
116 paleomagnetic directions obtained in this sequence, display either a record of a  
117 geomagnetic transition from reversed to normal polarity, likely the Gilbert-Gauss  
118 reversal, or a composite transition from chron C2Ar to subchron C2An-2n. Thus,  
119 another aim of this work is to analyze the paleointensity variation during such kind of  
120 record. From bottom to top of the volcanic sequence, the lava flows yielded 14  
121 reversed, one transitional, and 5 normal paleomagnetic directions. Both mean  
122 paleomagnetic poles of the stable polarity populations disagree with the expected pole  
123 position for their age but the possible occurrence of tectonic rotations has been ruled  
124 out (Sánchez-Moreno et al., 2018).

125

126 The paleointensity study on the Apnia sequence has been motivated by previous  
127 successful results in other basalt sequences of similar age in the Djavakheti region  
128 (South Georgia) (e.g. Borisova & Sologashvili, 1985; Calvo-Rathert et al., 2011, 2013;  
129 Camps et al., 1996; Goguitchaichvili et al., 2000, 2001, 2009, 2016). In spite of the  
130 excellent characteristics for obtaining paleointensities of this volcanic province;  
131 regarding the composition, morphology, formation and arrangement of lava flows, the

132 number of studies carried out is still scarce in comparison with other locations (e.g.  
133 Hawaii, Iceland or Galapagos). In addition, this sequence has a special interest due to  
134 the directional data obtained. The record shows normal and reverse polarities  
135 separated by a transitional one. Together with this directional record, the  
136 paleointensities obtained, provide information about the behavior of the Earth  
137 magnetic field during polarity changes. Likewise, the intensity values obtained help us  
138 to develop a more rigorous interpretation of the sequence, since the frequency in the  
139 flow emission is unknown and we cannot know at what specific moment the polarity  
140 reversal/s occurred during the time covered by the formation of such sequence.

141

142 As mentioned above, the choice of a multi-method approach is of special interest  
143 due to the need to obtain high reliability intensity data. When we analyze the global  
144 intensity database, we can see disagreements between data from similar locations and  
145 ages and a wide bias in the geographic distribution. Reliable data are necessary to  
146 understand how the intensity behaves during and near polarity changes, as well as  
147 during stable periods. Regarding the latter topic, the time-averaged value of the  
148 Earth's magnetic field strength is the subject of an ongoing intense discussion (e.g.  
149 Goguitchaichvili et al., 1999; Heller et al., 2002; Juarez & Tauxe, 2000; Lawrence et al.,  
150 2009; McFadden & McElhinny, 1982; Tanaka et al., 1995; Tauxe et al., 2013; Valet et  
151 al., 2005; Valet & Fournier, 2016; Wang et al., 2015).

## 152 **2. Geological setting**

153

154 The Apnia sequence (41° 21' 40" N, 43° 16' 02" E) was sampled in the volcanic  
155 Djavakheti Highland region, located in the central sector of the Lesser Caucasus (South  
156 Georgia) (Fig. 1.). This mountain range, which is included in the Alpine-Himalayan belt,  
157 is being generated by the still active collision of the Eurasian and Arabian plates.  
158 Within the so-called post-collision stage (Adamia et al., 2011) different stages of  
159 volcanic activity have taken place (Lebedev et al., 2008) in the Lesser Caucasus area.  
160 The volcanism that generates the materials under study corresponds to the 3.7-1.8 Ma  
161 phase. A large number of volcanic cones and fissure volcanoes owing to NW-SE and  
162 NE-SW extensional strike-slip structures, also developed by the compressional regime  
163 (Avagyan et al., 2010), characterize this phase. This volcanism shapes the Djhavakheti  
164 and Armenian plateaus and is known as the Akhalkalaki Formation in the Djhavakheti  
165 region (Maisuradze and Kuloshvili, 1999).

166

167 The Apnia sequence comprises 20 consecutive lava flows of tholeiitic basalts that  
168 were sampled from top (AP01) to base (AP20). Between 6 and 12 cores were taken  
169 from each successive flow with a portable water-cooled drill and were directly  
170 oriented in the field with both a solar and a magnetic compass and an inclinometer.  
171 The lowermost dated flow yields a K-Ar age ( $\pm 2\sigma$ ) of  $3.70 \pm 0.20$  Ma (flow AP11) and  
172 the uppermost one  $3.09 \pm 0.10$  Ma (flow AP01) (Lebedev et al., 2008). In addition, two  
173 more dates in flows AP05 and AP08 yield ages of  $3.28 \pm 0.10$  Ma and  $3.75 \pm 0.25$  Ma  
174 respectively (Lebedev et al., 2008). The Apnia sequence has been described in a

175 previous work as a record of a composite transition, either the Gilbert Gauss polarity  
176 reversal or a composite transition from chron C2Ar to subchron C2An-2n (Sánchez-  
177 Moreno et al., 2018).

### 178 **3. Rock magnetic and paleomagnetic results**

179

180 A comprehensive set of rock-magnetic experiments was carried out by Sánchez-  
181 Moreno et al. (2018) to determine the carriers of remanent magnetization, to obtain  
182 information about their thermal stability, and to estimate the magnetic domain state.  
183 These results are used here to select the most promising samples for paleointensity  
184 experiments.

185

186 Saturation magnetization vs. temperature (Ms-T) curves enabled to distinguish  
187 four different kinds of behavior (Fig. S3): i) Type H: Magnetic minerals are  
188 characterized by reversible curves with a single Curie temperature ( $T_C$ ) near to 580°C,  
189 corresponding to low-Ti titanomagnetite/magnetite. ii) Type H\*: A similar behavior to  
190 type-H samples, with the same low-Ti titanomagnetite phase. However, initial and final  
191 magnetizations differ by more than  $\pm 15\%$ . In some cases, a weak phase with  $T_C$  about  
192 615 °C is detectable. This observation might be attributed to the presence of oxidized  
193 magnetite (maghemitization). iii) Type L: This group displays irreversible behavior and  
194 two mineral phases. The first phase is observed in the heating curve between 190 °C  
195 and 280 °C and matches high-Ti titanomagnetite. The second one is a high  $T_C$  phase  
196 observed in both heating and cooling curves, which is interpreted again as low-Ti  
197 titanomagnetite, and represents only a tiny fraction of the initial magnetization. iv)  
198 Type M: It also shows an irreversible behavior and two phases can be distinguished,  
199 low-Ti titanomagnetite and an intermediate  $T_C$  phase within the 320 °C to 440 °C range  
200 in the heating curve.

201

202 Hysteresis parameters depicted in a Day plot show that the samples present a  
203 PSD-like magnetic behavior, which could also be interpreted as a mixture of single  
204 domain (SD) and multidomain (MD). We observe that hysteresis parameters have a  
205 certain trend towards MD grains. However, a recent study (Roberts et al., 2018) claims  
206 that the Day plots do not lead to a simple and direct inference on the domain states,  
207 due to the number of variables that influence the hysteresis curve values.

208

209 Thus, magnetic mineralogy experiments indicate a pseudo-single-domain (PSD)  
210 titanomagnetite with different titanium contents as the main carrier of magnetization  
211 (Sánchez-Moreno et al., 2018).

212

213 The analysis of paleomagnetic directions recovered from the Apnia volcanic  
214 sequence is consistent with a record of a polarity reversal having taken place between  
215 3 and 4 Ma (Sánchez-Moreno et al., 2018). A succession of 14 lava flows of reversed  
216 polarity is shown in the lower part, whose average pole differs from the expected one  
217 (Fig. S3). The reversed polarity flows are overlain by a single flow that has recorded a

218 transitional polarity, with an intermediate VGP latitude of 12.5°. On the top, 5 lava  
219 flows display normal polarity, with a mean pole further away from the expected pole  
220 than the mean pole of the reverse polarity section. However, the occurrence of  
221 tectonic rotations has been ruled out (Sánchez-Moreno et al., 2018). Therefore, a short  
222 recording time unable to average PSV and/or an anomalous Earth's magnetic field  
223 (EMF) record are both possible interpretations from the directional data of Apnia  
224 sequence (Sánchez-Moreno et al., 2018).

#### 225 **4. Polished thin sections analysis**

226

227 Polished thin sections have been analyzed with reflected light optical microscope  
228 and scanning electron microscope (SEM) in order to check the thermoremanent origin  
229 of the magnetization, as well as to characterize with more precision, the nature of the  
230 mineral carriers of remanence, regarding the textures, morphologies, distribution and  
231 sizes of the opaque minerals (i.e. mainly titanomagnetites, see section 3).

232

233 Based on the different behaviors of the Ms-T curves, five samples from the Apnia  
234 sequence were selected, two from type H and one of each type H\*, M and L. The  
235 reflected light optical microscopy was carried out in Géosciences Montpellier  
236 (Université de Montpellier, France) with a Leitz Orthoplan Microscope. Elaboration of  
237 the polished thin sections, backscattered images and composition analyzes were  
238 obtained at Universidad del País Vasco (UPV/EHU, Bilbao, Spain). The polished thin  
239 sections were carbon coated and analyzed with a JEOL JSM-7000F SEM equipped with  
240 an Oxford Inca Pentafet X3 energy dispersive X-ray analyzer (EDX). The EDX  
241 microanalyzes were performed with a backscattered electron signal (BSE) at 20 kV and  
242 a current intensity of  $1 \times 10^{-9}$  A, with a working distance of 10 mm.

243

244 The samples are holocrystalline with micro-porphyric and trachytic textures with  
245 vesicles of variable size. They comprise plagioclase, olivine, clinopyroxene, and opaque  
246 minerals, as an overall petrological description of the Apnia section. Dominant opaque  
247 phases are titanomagnetites and ilmenites with different degrees of oxi-exsolution or  
248 intergrowths.

249

250 Based on the textures, distribution and sizes of the opaque minerals, two groups  
251 of samples can be distinguished: one characterized by the presence of euhedral to  
252 subeuhedral crystals with maximum sizes of 140  $\mu\text{m}$  (samples AP02 and AP06; Fig. 1.a  
253 and 3.a); and a second one with anhedral opaque minerals with skeletal and dendritic  
254 growth morphologies and maximum crystal sizes of 75  $\mu\text{m}$  (samples AP08, AP13 and  
255 AP14; Fig. 2.d), corresponding to quick quenching sectors of the lava flows. In the  
256 former group there are homogeneous, non-exsolved, titanomagnetite crystals as well  
257 as titanomagnetites with dense ilmenite intergrowths of Trellis and Sandwich types  
258 (Fig. 1.c, d, e and 2.b). According to Haggerty (1991) these intergrowths correspond to  
259 textural stages C1 to C3 of high temperature (>600°C) oxidation of titanomagnetite.  
260 Frequently in basalts, ilmenite and magnetite exsolution is likely produced by oxidation

261 above titanomagnetite  $T_C$  during rock formation. This process indicates that original  
262 TRM is most likely recorded. Ilmenite crystals also show evidences of oxidation due to  
263 the presence of fine ferrian-rutile needles (Fig. 1.c) indicative of an oxidation stage R2  
264 (Haggerty, 1991). Moreover, sample AP06 shows several titanomagnetite crystals  
265 undergoing maghemitization along the margins (Fig. 1.b and 2.b), as a product of low-  
266 temperature oxidation (<300°C). This process is related to the high  $T_C$  observed in the  
267  $M_S$ -T curves. In the latter group, the titanomagnetites show abundant Trellis and  
268 Sandwich types of ilmenite intergrowths (Fig. 1.c, d, e and 2.e) categorized as C3  
269 textural stage of oxidation according to Haggerty, (1991). Furthermore, sample AP08  
270 shows small euhedral Ti-poor titanomagnetites in disseminated form (Fig. 1.f and 2.f).

271

272 The process of ilmenite intergrowths on titanomagnetites, on the one hand,  
273 generates titanomagnetite grains up to 100 times smaller than the original grain,  
274 which provides more stable SD grains for the determination of paleointensities. On the  
275 other hand, it allows the verification of a high temperature (above Curie temperature)  
276 remanence acquisition, suitable for the type of studies that are carried out in this  
277 work. The observed maghemitization is an oxidation process at low temperature  
278 produced in later stages when the lava is cooling or is already cold. It indicates a  
279 probable secondary magnetization that can blur the direction and the intensity  
280 determination. Consequently, the samples where maghemitization is observed are  
281 discarded for paleointensity experiments.

## 282 5. Paleointensity methods

283

284 In the present study, paleointensity determinations have been performed with  
285 the multispecimen technique without corrections (MSP-DB) (Biggin and Poidras, 2006;  
286 Dekkers and Böhnell, 2006) and with corrections (MSP-FC and MSP-DSC) (Fabian and  
287 Leonhardt, 2010) at the palaeomagnetic laboratory of UNAM in Morelia (Mexico) and  
288 the palaeomagnetic laboratory of Géosciences Montpellier (France). In addition,  
289 specific selection criteria (Leonhardt et al., 2004; Paterson et al., 2014 ) have been  
290 applied to intensity values obtained in a previous study (Sánchez-Moreno et al., 2020)  
291 on the same flows with the Thellier-Thellier (TT) (Thellier and Thellier, 1959) and IZZI  
292 (Yu et al., 2004) methods. Subsequently, they have been jointly analyzed with the  
293 results from the MSP determinations. The main motivation of this double approach  
294 was to provide an additional strong reliability check with a multi-method consistency  
295 test. On the other hand, this kind of analysis can also help to evaluate the performance  
296 of the MSP method.

297

### 298 5.1. Multispecimen methods

299

300 The *multispecimen parallel differential pTRM* method (MSP-DB) (Biggin and  
301 Poidras, 2006; Dekkers and Böhnell, 2006) was proposed as a technique fitted to  
302 estimating paleointensities independently of domain states of magnetic minerals.  
303 Different fields ( $B_{lab}$ ) are applied to several sister specimens of each sample, parallel to

304 the original NRM (TRM) and at the same temperature. The temperature is chosen to  
305 avoid magneto-chemical transformations, but it must be sufficient to create a TRM  
306 spanning an adequate fraction for the paleointensity determination. Therefore, the  
307 method provides two advantages over the Thellier type: 1) The magnetic history  
308 effects are eliminated if the independence over the domain state structure is assumed.  
309 2) The number of heatings is drastically reduced and the temperature applied is  
310 selected to avoid magneto-chemical alterations. Correction steps have been  
311 introduced in order to avoid the possible paleointensity overestimation observed in  
312 some previous studies (Fabian and Leonhardt, 2007; Michalk et al., 2008, 2010; Calvo-  
313 Rathert et al., 2016) on lavas containing a significant MD fraction, questioning the  
314 theoretical model first introduced by Biggin and Poidras, (2006). The complete  
315 *multispecimen - domain state correction* protocol (MSP-DSC) (Fabian and Leonhardt,  
316 2010) includes the same steps as the original MSP-DB method with three additional  
317 heating-cooling cycles. The new steps allow for the correction of the TRM fraction  
318 involved in the determination (MSP-FC), reducing the pTRM-tail effect from MD grains  
319 (MSP-DSC), and the calculation of the relative alteration produced (see Table S2.).

320

321 Measurements were carried out in two different laboratories: *Servicio*  
322 *Arqueomagnético Nacional – Instituto de Geofísica Unidad Michoacaán (IGUM) -*  
323 *Universidad Nacional Autónoma de México (UNAM)* and *Géosciences - Université de*  
324 *Montpellier (France)*. The online version Multispecimen Paleointensity 1.5. software  
325 (online version [http://ambre.gm.univ-montp2.fr/camps/MSP\\_DSC/](http://ambre.gm.univ-montp2.fr/camps/MSP_DSC/)) has been used for  
326 the interpretation of MSP results.

327

328 The sample pre-selection criteria in the UNAM laboratory were the following: a  
329 univectorial ChRM component, the presence of reversible Ms-T curves (H and H\*  
330 types), a median destructive field (MDF) > 25  $\mu\text{T}$  in alternating field (AF)  
331 demagnetizations and magnetization drops at high temperatures in the thermal  
332 demagnetization experiments. The chosen temperature was 450°C, at which 75% of  
333 the magnetization still remains.  $B_{\text{lab}}$  was applied at intervals of 5 or 10  $\mu\text{T}$ , according to  
334 the results being obtained, within a range of 5/10  $\mu\text{T}$  to 80  $\mu\text{T}$ , on 7 specimens from  
335 each studied lava flow for the MSP-DB protocol and on 4 to 5 specimens for the MSP-  
336 DSC protocol. Small irregular fragments were taken from standard samples and  
337 prepared in 10cm<sup>3</sup>-standard size salt pellets. The salt samples were placed in a mu-  
338 metal home-made sample holder, heated with the TD48-DC (ASC) thermal  
339 demagnetizer, and measured with a JR-6 spinner magnetometer (AGICO).

340

341 In Géosciences – Montpellier, the samples were chosen under the same pre-  
342 selection criteria as in UNAM. In addition, the specimens of the same core had to show  
343 Arai plots without negative pTRM checks in previously performed Thellier-type  
344 experiments (Sánchez-Moreno et al., 2020). The heating temperature was also set at  
345 450°C. At this temperature the selected samples still retain between 20% and 80% of  
346 the TRM in the Thellier-type experiments and it is low enough to avoid magneto-  
347 chemical alteration.  $B_{\text{lab}}$  was applied in intervals of 10  $\mu\text{T}$ , from 10  $\mu\text{T}$  to 80  $\mu\text{T}$ , to 8

348 specimens from each selected lava flow. Small irregular fragments were taken from  
349 standard samples and were prepared in 10-cm<sup>3</sup>-standard size plaster. The samples  
350 were heated in the FURÉMAG prototype furnace (Patent # 1256194). A precise  
351 magnetic induction field, perfectly controlled in 3D with a precision better than 1°, was  
352 applied to each sample during heating and/or cooling. Fanjat (2012) showed that it is  
353 not necessary to apply a cooling rate correction with the MSP protocol (Tema et al.,  
354 2015) during the test and the calibration of this furnace. Measurements were  
355 performed with a superconducting magnetometer (2G Enterprise).

356

357         When the sample's individual declination and inclination measured at different  
358 steps was found different to the original NRM, they were not corrected, as it is  
359 impossible to apply a correction to the angle due to pTRM-tails caused by MD grains.  
360 However, when the maximum angle between the NRM after pTRM acquisition and the  
361 total NRM exceeded a critical angle of 10°, the measurement for that specimen was  
362 dismissed. Parameter  $\alpha$  (Fabian and Leonhardt, 2010) is a constant to calculate the  
363 contribution of the domain state effect, used to avoid a possible overestimate of the  
364 domain-state contribution. In this work an  $\alpha = 0.5$  value is taken for the calculations. A  
365 set of criteria based on the linear regression analysis and correction ratio  $Q_{DB}$ ,  $Q_{FC}$  and  
366  $Q_{DSC}$  calculations (Fabian and Leonhardt, 2010) under MSP-DB, MSP-FC and MSP-DSC  
367 protocols, was used to select the individual MSP data and reject those of poor  
368 technical quality (Table S3).

369

## 370         **5.2. Multispecimen results**

371

372         Seven MSP determinations on single cores belonging to 7 different lava flows  
373 were measured in the UNAM laboratory and 5 MSP determinations were carried out  
374 on samples from 5 different lava flows in Géosciences – Montpellier. In this latter case,  
375 the specimens for each determination were taken from a single core in 3 cases, and  
376 from different but nearby cores in 2 cases (cores 03 and 04 separated 40 cm in AP01  
377 and cores 07 and 09 separated 2 m in AP20). In all, MSP paleointensity determinations  
378 could be performed on 12 of the 20 flows comprising the Apnia sequence. Table S1  
379 shows the quality criteria used to select successful paleointensity determinations. Two  
380 sets of threshold values of different stringency were chosen to distinguish between  
381 two different determination quality levels, class A and class B (Table S3). After  
382 applying the proposed threshold criteria, 6 MSP-DB determinations from a total of 12  
383 are considered as reliable (Table 1), all of them belonging to class B. The determination  
384 obtained for flow AP03, however, shows a high relative error  $\Delta B$  ( $\Delta H$  from Fabian and  
385 Leonhardt, (2010), Table S1). Because AP03 meets all remaining criteria, it has been  
386 labeled as class B\*. It should be mentioned that error parameters  $\epsilon_{alt}$  (and also  $\Delta B$ )  
387 may, in theory, also be applied to MSP-DB. Although they cannot be calculated for the  
388 MSP-DB protocol, the same processes that generates these errors in the MSP-DSC  
389 experiments, also occur in MSP-DB because the temperature attained is the same.

390

391 Eight successful determinations were obtained with the MSP-DSC protocol, (67%  
392 success rate) 2 of them belonging to class A, five to class B and sample AP03 again to  
393 B\*(Fig. 3 and Table 3). Paleointensities obtained under the MSP-DB protocol range  
394 between 14 and 67  $\mu\text{T}$ , while MSP-DSC paleointensities yield values between 14 and 55  
395  $\mu\text{T}$ , except for AP05, which despite passing all quality criteria, yields an apparently  
396 more anomalous value of 100  $\mu\text{T}$  (Table 1).

397

398 Another interesting result arising from the comparison of the *multispecimen*  
399 *parallel differential pTRM method* (MSP-DB) (Biggin and Poidras, 2006; Dekkers and  
400 Böhnel, 2006), *multispecimen - fraction correction* (MSP-FC) and *multispecimen -*  
401 *domain state correction* (MSP-DSC) (Fabian and Leonhardt, 2010) protocols, is their  
402 relationship in terms of the paleointensity value. In previous works, an overestimation  
403 of DB over DSC paleointensities of up to 20% was observed (Fabian and Leonhardt,  
404 2007; Michalk et al., 2008, 2010; Calvo-Rathert et al., 2016). In this work, DSC  
405 paleointensities weaker than DB ones have been obtained in all determinations, except  
406 in AP20, where intensities  $\text{FC} > \text{DSC} > \text{DB}$ . In AP14 DB, FC and DSC values are  
407 indistinguishable.

408

### 409 **5.3. Thellier-type determinations**

410

411 In a previous study (Sánchez-Moreno et al., 2020), Thellier-type paleointensity  
412 determinations with the original Thellier-Thellier (TT) protocol (Thellier and Thellier,  
413 1959) and the IZZI protocol (Yu et al., 2004) have been performed on samples from all  
414 20 flows of the Apnia sequence. TT experiments were carried out in the paleomagnetic  
415 laboratory of the University of Burgos on small cylindrical specimens of 8 mm diameter  
416 with a TD48-SC (ASC) thermal demagnetizer under argon atmosphere. IZZI experiments  
417 were carried out in the paleomagnetic laboratory of the Scripps Institution of  
418 Oceanography, UCSD (USA) with specimens prepared as small irregular fragments in 10  
419 mm diameter vials. Experiments were performed in a homemade single chamber  
420 thermal demagnetizer under air. In both cases, laboratory field  $B_{\text{lab}}$  was set at 40  $\mu\text{T}$   
421 and several pTRM checks were performed.

422

423 The Thellier GUI PmagPy package software (Tauxe et al., 2016) was used for the  
424 interpretation of results obtained with both protocols. A set of especially strict  
425 selection criteria (Tauxe et al., 2016) was used to assess the quality of the experiment  
426 conditions, the absence of alterations and the amount of magnetization carried by  
427 multidomain grains (MD). Application of this very strict set of criteria yielded 4 out of  
428 55 reliable absolute paleointensity determinations with the TT method and 41 out of  
429 100 with the IZZI method, yielding paleointensity results in 8 of 20 studied lava flows at  
430 the site level. At the reverse polarity lower Apnia section, low VADM values between  
431 2.9 and  $4.6 \times 10^{22} \text{ Am}^2$  were obtained, while the normal polarity upper section  
432 displayed a single value of  $5.6 \times 10^{22} \text{ Am}^2$ . All these paleointensity values lie well below  
433 the present-day dipole moment in Georgia ( $8.4 \times 10^{22} \text{ Am}^2$ ).

434

435 One of the aims of the present study was to provide an additional reliability  
436 check with a multi-method consistency test. A positive consistency test would ensure  
437 the reliability of determinations retrieved from Thellier-type and MSP determinations  
438 with matching paleointensity values (e. g. Monster et al., 2015a; Calvo-Rathert et al.,  
439 2016; De Groot et al., 2016)., as a match obtained from two failed experiments  
440 performed with different methods would be highly unlikely. In fact, Biggin and  
441 Paterson, (2014) suggest that the average per site must include paleointensities from  
442 more than one technique. A first condition to perform a comparison between Thellier-  
443 type and MSP results is that both have been obtained from successful determinations.  
444 As mentioned above, selection criteria applied by Sánchez-Moreno et al. (2020) were  
445 especially strict. However, when the multi-method consistency test is applied, it would  
446 be not necessary that parameters of selection criteria for the Thellier-type  
447 experiments are so strict. On one hand, although it is still necessary that the final  
448 results are able to stand by themselves, the multi-method consistency check can  
449 provide an additional confirmation of the results. In addition, as noted by Patterson et  
450 al. (2014), some set of criteria can be too strict, as they lead to the rejection of ideal  
451 samples subject to experimental noise. For this reason, we have performed a new  
452 interpretation of our experimental Thellier-type determinations (Table S4 and S5), not  
453 using the criteria of Tauxe et al.(2016), but the still reliable and commonly used  
454 ThellierTool criteria (Leonhardt et al., 2004) as modified by Paterson et al. (2014),  
455 allowing two quality levels A and B (Table S2), in order to perform a multimethod  
456 consistency check together with the results obtained with the MSP determinations  
457 from the present study.

## 458 **6. Discussion**

459  
460 One of the aims of the present work is to analyze the paleointensity variation  
461 along a lava flow sequence including a polarity transition. For this analysis, reliable  
462 paleointensity data, ideally for each lava flow are needed. The comparison of the  
463 results obtained from the different types of paleointensity determination experiments  
464 may reinforce their reliability. Two different Thellier-type methods (Thellier-Thellier  
465 and IZZI) and the MSP method including three different protocols including corrections  
466 have been considered. There is a general agreement among the paleomagnetic  
467 community that Thellier-type methods should be considered as the most reliable ones  
468 because of their robust physical basis. MSP methods, however, are more recent and  
469 still need to be substantiated, for which a greater number of data is needed. To  
470 accomplish these goals, the rationale of the multi-method approach used in the  
471 present study has been the following:

- 472
- 473 (i) Results of both Thellier-type and multispecimen determinations are obtained after  
474 applying specific selection criteria to select reliable paleointensity determinations.
  - 475 (ii) Successful Thellier-type paleointensity determinations are used to evaluate the  
476 quality of multispecimen determinations, as Thellier-type methods are considered the  
477 most reliable.

478 (iii) Agreement of paleointensity results from multispecimen and Thellier-type  
479 determinations is considered as an added strong indicator of a successful  
480 paleointensity determination, as a match obtained from two failed experiments  
481 performed with different methods can be considered highly unlikely.

482

483 MSP results and some criteria used to select them will be discussed in the  
484 following sections.

485

### 486 **6.1. MSP method and quality criteria**

487

488 The fraction range  $f$  (Fabian and Leonhardt, 2010) is the ratio between the  
489 fraction of NRM removed and overprinted by the laboratory pTRM for each point, i. e.  
490 for each specimen subjected to a different  $B_{lab}$ . The commonly proposed threshold  
491 values lie between 0.2 and 0.8 (20% and 80% of the total NRM). In this interval, the  
492 fraction is large enough to be accurately measured and still clearly below a total TRM  
493 (Tema et al., 2016). It is obtained from the half vector sum between measurements  $m_1$   
494 and  $m_2$  of the MSP-DSC procedure (Table S2) normalized by the NRM, and for this  
495 reason it can only be calculated for the FC and DSC determinations. Even so, we  
496 consider that it is also applicable to the original DB method, because it depends on the  
497 temperature reached during the experiment (and therefore on the amount of TRM  
498 unblocked and overprinted), which in the three MSP variants is the same. In the  
499 present study, it was decided to apply 450°C to all samples, but in some  
500 determinations,  $f$  is less than 0.2. In such cases, a higher temperature would have been  
501 more adequate, since the magnetization drop in these samples occurs at slightly higher  
502 temperatures, and the  $f$ -range used in the MSP experiments is sensitive to the  
503 temperature applied. Comparison with Thellier-type experiments, however, shows  
504 that some determinations in which  $f < 0.2$  (AP11, AP15 and AP19) yield similar  
505 paleointensities (see section 7.2.). This observation may indicate that a lower  $f$  range  
506 may be valid in MSP in some specific cases. In the present study, these three  
507 determinations have not been formally considered reliable MSP determinations in  
508 Table 1, but their agreement with Thellier-type results (see discussion below) has  
509 driven us to consider them for final paleointensity calculations. In Table 1 they have  
510 been named as Thellier-validated ( $T^V$ ) results.

511

512 The average alteration error  $\epsilon_{alt}$  (Fabian and Leonhardt, 2010) is also one of the  
513 new quality criteria used in the MSP-DSC protocol. It is calculated with measurement  
514  $m_1$  and repeated measurement  $m_4$  of the of the MSP-DSC procedure (Table S2). As it  
515 is considered that for thermo-chemical changes the temperature attained is more  
516 important than the number of heatings, it is possible to use  $\epsilon_{alt}$  for all MSP variants.  
517 Monster et al., (2015a and b) have proposed a strict threshold of 3%, which is used by  
518 Calvo-Rathert et al., (2016), while Tema et al., (2016) take a more flexible 10%.  
519 Comparing the obtained MSP paleointensity values with the Thellier-type ones (as will  
520 be discussed in the next section) and analyzing their coincidences, in this work 10% is  
521 used for class A and 15% for class B determinations.

522

523 Parameters  $\Delta B$  ( $\Delta H$  from Fabian and Leonhardt, 2010) and  $CI_{95}$  (see  
524 Multispecimen Paleointensity 1.5. software online version <http://ambre.gm.univ->  
525 montp2.fr) provide an estimation of the uncertainty.  $CI_{95}$  is the bootstrapped 95%  
526 confidence interval calculated and critically evaluated with the Shapiro-Wilk test of  
527 normality (see MultiSpecimen Paleointensity software online version  
528 [http://ambre.gm.univ-montp2.fr/camps/MSP\\_DSC/](http://ambre.gm.univ-montp2.fr/camps/MSP_DSC/)). It is in reasonably good  
529 agreement and within the error bar compared to the value obtained with the  
530 conventional Thellier protocol (Tema et al., 2015). An almost ideal determination is  
531 achieved when the upper and lower limits are symmetrical with respect to the  
532 paleointensity value.  $\Delta B$  is the final error of the determination obtained by the total  
533 error of each specimen used in the determination (see  $\Delta Q_i$  in Table S3). To find out  $\Delta B$ ,  
534 the alteration-induced error (which includes  $\varepsilon_{alt}$ ) and the approximation of the  
535 absolute error of the domain-state correction are calculated. Like the relative  
536 alteration error  $\varepsilon_{alt}$ ,  $\Delta B$  also depends on the temperature reached, and hence it may be  
537 considered to evaluate the quality of DB and FC determinations as well as those of the  
538 DSC. In the present study, the results provided in several cases by  $CI_{95}$  and  $\Delta B$  are  
539 contradictory. In such cases, only the  $CI_{95}$  parameter is taken into account.

540

## 541 **6.2. MSP vs. Thellier-type**

542

543 In this section, the agreement between mean flow paleointensities obtained with  
544 Thellier-type and MSP methods will be analyzed. For this comparison, and later  
545 calculation of the final flow-average paleointensities (Table 3), the results obtained  
546 with the DSC protocol have been considered as more reliable (see section 6.3) than  
547 those obtained with the MSP-DB protocol. It must be noted that some MSP-DSC  
548 paleointensities do not pass all quality criteria but agree with those obtained with  
549 Thellier-type methods

550

551 All flows have been grouped according to the agreement of their MSP-DSC and  
552 Thellier-type paleointensity results together with their technical quality. For this  
553 classification, we assume that TT-IZZI and MSP-DSC mean paleointensities agree if the  
554 difference between them is less than  $8 \mu T$ . The use of relative differences to quantify  
555 the agreement of results in the lower section implies too small errors when compared  
556 to the experimental results. Consequently, a standard value has been chosen. In this  
557 case, it is 15% of the present-day field in Georgia ( $50 \mu T$ ), which is approximately  $8 \mu T$ .  
558 The problem of applying the same percentage to both low and high paleointensities is  
559 discussed in Tauxe and Staudigel, (2004) and Tauxe, (2006). The following types of  
560 behavior can be distinguished:

561

562 Class 1. Good technical quality MSP-DSC paleointensities agree with Thellier-type ones:  
563 This case is observed for flows AP01, AP14 and AP17.

564

565 Class 2. Good technical quality MSP-DSC paleointensities disagree with Thellier-type  
566 ones: This case happens in flows AP03, AP04, AP05, AP10 and AP12. Here, MSP-DSC  
567 determinations are rejected because the reliability of Thellier-type methods over MSP  
568 is *a priori* assumed. In addition, the Thellier-type determinations are based on a  
569 greater number of determinations.

570

571 Class 3. Bad quality MSP-DSC paleointensities agree with Thellier-type ones: This case  
572 could be observed in flows AP11, AP15, AP19 and AP20. In such case MSP-DSC data  
573 support the reliability of Thellier-type results. This case may raise doubts about the  
574 chosen threshold values from the quality parameters used (see section 7). Only AP11  
575 and AP19 do not fit the quality criterion  $f$ . As discussed in the previous section, we  
576 consider them reliable with  $f < 0.2$ .

577

578 The comparison of results obtained from MSP and Thellier methods can also  
579 supply interesting information regarding the supposed ability of the first one to  
580 provide successful results. Especially in those cases when TT or IZZI display concave-up-  
581 shape Arai plots which are not able to deliver reliable paleointensity results. For flow  
582 AP01, specimens from two different samples (03A and 04A) have been used in an MSP-  
583 DSC determination, which pass the quality criteria. In a specimen of the same sample  
584 03A, an IZZI determination with a concave-up shape Arai plot was detected. Specimen  
585 04A, on the other hand, shows a linear-shape Arai plot, but a MD trend in the Day-plot.  
586 In flow AP05, sample 01B displays a concave-up-shaped Arai plot and a successful  
587 MSP-DSC determination. Therefore, we believe that the MSP-DSC determination  
588 behaved independently of the domain state in these samples.

589

590 Biggin and Paterson, (2014) suggest that a site-average must include  
591 paleointensities from more than one technique to support results of high reliability. In  
592 addition, they propose a new set of largely qualitative reliability criteria for  
593 paleointensity results at the site mean level, which they term  $Q_{PI}$ . They intend to  
594 identify biasing agents applicable to paleointensity measurements which are  
595 sometimes obviated to quantify the reliability of the paleointensity values obtained  
596 from a study. The  $Q_{PI}$  criteria and the fit of our results to them are the following:

597

- 598 1. AGE: Apnia paleointensity results show a reliable age and paleomagnetic  
599 behavior derived from a primary component of remanence.
- 600 2. STAT: 10 lava flows passed the requirement of 5 individual specimens used in the  
601 average paleointensity (AP01, 02, 04, 11, 14, 16, 17, 18, 20 and 19). It is worth  
602 mentioning that 5 flows have 3 or 4 specimens in the average (AP05, 06, 07, 09,  
603 and 13), as commonly, 3 paleointensity determinations are considered a good  
604 average.
- 605 3. TRM: Microscope analysis supports the evidence that the remanence is a  
606 thermoremanence.
- 607 4. ALT: pTRM checks and rock mag experiments (also  $\epsilon_{alt}$  parameter in MSP)  
608 support that there is not alteration.

- 609 5. MD: A high  $f$  parameter in Thellier-type and domain state correction in MSP-DSC  
610 determinations verify that the MD effect does not affect the final paleointensity  
611 estimate.
- 612 6. ACN (Anisotropy of TRM, Cooling rate and Non-linear TRM effects):
- 613 - Anisotropy of TRM: Anisotropy of magnetic susceptibility (AMS) was  
614 measured on one sample from each flow showing a corrected anisotropy  $P'$   
615 value (Jelinek, 1981) of approximately 4% ( $P'$  between 1 and 1.040, average  
616 1.014, Sánchez-Moreno et al., 2020?). The gamma statistic  $\gamma$  (Paterson et al.,  
617 2014) in both the Thellier-Thellier and IZZI determinations yields values  
618 between  $0.2^\circ$  and  $3.7^\circ$ . Only when  $\gamma \gg 4^\circ$  it is considered that there is a  
619 higher chance that the specimen is anisotropic (Paterson et al., 2015).
  - 620 - Cooling rate: The lava flows characteristics (thickness, composition, etc.) allow  
621 the assumption that the cooling-rate does not affect the paleointensity  
622 experiments, given that it does not vary significantly in the range of thickness  
623 of the individual cooling units. The Thellier-Thellier and IZZI experiments have  
624 been performed by cooling the samples under natural conditions ( $\sim 10$ h) and  
625 with a fan ( $\sim 1$ h) respectively (Sánchez-Moreno et al., 2020), without  
626 differences in the results.
  - 627 - Non-linear TRM effects: They are minimal when the laboratory and ancient  
628 field strengths are approximately equal (Paterson, 2013; Selkin et al., 2007).  
629 For most typical geological materials (i. e., lavas), if both fields are within  $\sim 1.5$   
630 times each other, the influence of non-linear TRM is likely to be minimal  
631 (Biggin and Paterson, 2014).
- 632 7. TECH: Final paleointensity from 11 lava flows have been calculated from more  
633 than one technique (AP01, 02, 04, 07, 11, 13, 14, 17, 18, 20 and 19).
- 634 8. LITH: The paleointensity estimations have been performed over samples of  
635 similar lithology and with similar unblocking behavior.

636

637 From this analysis 10 final mean paleointensities (lava flows AP01, 02, 04, 11, 14,  
638 16, 17, 18, 20 and 19) can be classified as  $Q_{PI} = 7$ . AP07 and AP13 show a  $Q_{PI} = 6$ . Lastly,  
639 the 8 remaining final mean paleointensities have  $Q_{PI} = 5$ .

640

### 641 **6.3. Paleointensity average per lava flow**

642

643 As mentioned above, three different types of paleointensity determinations  
644 have been used and results show a rather large variability. Now, the question of how  
645 to calculate an average intensity per lava flow that is reliable and representative is  
646 raised. It should be considered that the paleointensity for each lava flow has been  
647 averaged for each method if determinations passed the proposed quality thresholds.  
648 In addition, for MSP-DSC determinations, the agreement with Thellier-type results is  
649 considered as decisive. In doubtful cases, the agreement with paleointensities  
650 obtained in adjoining flows is also taken into account. Mean paleointensities have  
651 been weighted according to the number of determinations of each method (Table 3),  
652 and the valid average paleointensity per flow must have a standard deviation value

653 within  $\pm 25\%$ . According to the methods involved in the average, various quality levels  
654 can be distinguished.

655

656 Quality 1: Average paleointensity per lava flow calculated with at least one Thellier-  
657 type determination and one MSP-DSC determination of good quality and matching  
658 Thellier results. Flows AP01, AP14 and AP17 present the most reliable paleointensities  
659 (Table 3) yielding quality 1 results.

660

661 Quality 2: Three or more TT and IZZI determinations comprise the average.  
662 Alternatively, at least a single Thellier-type determination and an MSP-DSC  
663 determination that do not reach all quality thresholds but match the results obtained  
664 with the Thellier method (AP11, AP15, AP19 and AP20). In this latter case, the average  
665 paleointensity has been calculated without MSP-DSC (Table 3). In total, nine Quality 2  
666 determinations have been obtained.

667

668 Quality 3: Three or more determinations of a single Thellier-type method.  
669 Alternatively, a reliable MSP determination together with a Thellier-type experiment  
670 yielding a concave up Arai plot. However, no reliable MSP determinations  
671 accompanied by a concave up Arai plot were obtained in all the sequence. MSP-DSC  
672 results from AP05 yielded acceptable quality parameters, but the paleointensity value  
673 obtained displays an abnormally strong value, which clearly disagrees with the Thellier-  
674 type results. Therefore, this value has been discarded and only the average obtained  
675 from 4 IZZI determinations has been selected in AP05.

676

677 Quality 4: Less than three determinations of a single Thellier-type method. They are  
678 taken into account if they match the adjacent lava flow paleointensities, as is the case  
679 of AP03, AP08, AP10 and AP12. Flow AP03 might present the most questionable result  
680 because it has been obtained from a single Thellier-Thellier determination.  
681 Nevertheless, it agrees with the results from the adjacent flows.

682

683 Finally, average paleointensities have been obtained for all the 20 flows that  
684 comprise the Apnia sequence (Table 3 and Fig. 3). Three paleointensities belong to  
685 quality level 1, nine to quality 2, four to quality 3 and four to quality 4. Paleointensity  
686 values in the lower section of reverse polarity range between  $12.5 \mu\text{T}$  and  $24.6 \mu\text{T}$ . The  
687 intermediate polarity flow gives a value of  $25.2 \mu\text{T}$ . In the upper section of normal  
688 polarity, the paleointensities show higher values, which range between  $29.9 \mu\text{T}$  and  
689  $41.5 \mu\text{T}$ . The virtual axial dipole moment (VADM) has also been calculated for the final  
690 average paleointensities (Table 2, yielding values of between  $2.1$  and  $4.1 \times 10^{22} \text{ Am}^2$  in  
691 the reverse polarity part,  $4.3 \times 10^{22} \text{ Am}^2$  in the transitional polarity flow and in the  
692 normal polarity section between  $5.1$  and  $7.1 \times 10^{22} \text{ Am}^2$ .

693

694 **6.4. Directional results vs. paleointensities**

695

696 Paleomagnetic directions obtained in Apnia lava sequence are consistent with a  
697 record of a polarity reversal (Sánchez-Moreno et al., 2018). According to radiometric  
698 ages (Lebedev et al., 2008), the record may correspond either to the Gilbert-Gauss  
699 reversal (C2Ar to C2An-3n) or to a composite transition record from C2Ar to C2An-2n  
700 subchrons (Fig. S3). Moreover, Sánchez-Moreno et al. (2018) concluded that the  
701 analysis of paleomagnetic directions in combination with the virtual geomagnetic pole  
702 scatter and a few previously available paleointensity results (Calvo-Rathert et al.,  
703 2013), enable two non-exclusive interpretations: an anomalous EMF record or a short  
704 recording time unable to average paleosecular variation. As mentioned above, the  
705 flow-average paleointensities obtained in the present study range from 12.5 to 24.6  $\mu\text{T}$   
706 in the lower reverse-polarity section, the transitional flow yields 25.2  $\mu\text{T}$  and the upper  
707 normal-polarity section provide higher values between 29.9 and 41.5  $\mu\text{T}$ . All obtained  
708 intensity values are below the present field strength in Georgia (about 50  $\mu\text{T}$ ). During  
709 large departures of the geomagnetic field from the GAD, the intensity decreases  
710 significantly (e.g., Laj and Channell, 2007 and references therein). Furthermore, the  
711 intensity variation begins before the direction variation (Prévot et al., 1985a; Prévot et  
712 al., 1985b; Herrero-Bervera and Valet, 1999; Riisager et al., 2000). Under these  
713 circumstances, it is possible to interpret that the lower part of the Apnia sequence  
714 records the initial stage of the reversal, whereas the upper section shows the recovery  
715 of the EMF intensity, after the polarity transition.

716

717 The multi-method approach applied in the present study provides consistent  
718 paleointensity results in all flows of the sequence, allowing to support the previous  
719 directional interpretation of the record as a polarity reversal. It is, however, an  
720 arduous methodology which involves carrying at least two types of experiments. In  
721 comparison with other approaches to obtain high quality paleointensities, such as  
722 applying very strict selection criteria to Thellier-type determinations (Tauxe et al.,  
723 2016) which is less laborious, a higher number of reliable data might be obtained from  
724 the same data population (Sanchez-Moreno et al., 2020).

725

## 726 **7. Conclusions**

727

728 An inter-laboratory and multi-method absolute paleointensity determination  
729 study has been carried out on the Pliocene Apnia sequence that is composed of 20  
730 consecutive lava flows. According to paleomagnetic directions and available  
731 radiometric ages, the sequence seems to record either the Gilbert-Gauss reversal or a  
732 composite polarity transition from chron C2Ar to subchron C2An-2n (Sánchez-Moreno  
733 et al., 2018). Moreover, paleomagnetic results of the reverse polarity section provide  
734 two different but not conflicting interpretations: a relatively short recording time  
735 unable to average PSV and/or an anomalous EMF record (Sánchez-Moreno et al.,  
736 2018).

737

738 Absolute intensity determinations with the multispecimen technique were  
739 performed on 12 samples with both the original method (MSP-DB, Biggin and Poidras,  
740 2006; Dekkers and Böhnelt, 2006) and the extended protocol with corrections (fraction  
741 correction FC and domain state correction DSC; Fabian and Leonhardt, 2010). Eight  
742 MSP-DSC determinations from eight flows passed the proposed quality criteria.  
743

744 In a previous study (Sánchez-Moreno et al., 2020), Thellier-type paleointensity  
745 determinations with the original Thellier-Thellier (TT) (Thellier and Thellier, 1959) and  
746 the IZZI protocol (Yu et al., 2004) had been performed on samples from all 20 flows of  
747 the Apnia sequence, yielding paleointensity results in 8 of 20 studied lava flows. One of  
748 the aims of the present study was to provide an additional reliability check with a  
749 multi-method consistency test including results from both Thellier-type and MSP  
750 determinations. For this reason, we have performed a new interpretation of these  
751 experimental Thellier-type determinations with the commonly used ThellierTool  
752 criteria (Leonhardt et al., 2004) as modified by Patterson et al. (2014), in order to  
753 perform a multimethod consistency check together with the results obtained with the  
754 MSP determinations from the present study.  
755

756 Paleointensity results could be obtained in all 20 lava flows, and 11 flow averages  
757 are supported on different methods. The flow-average paleointensities obtained this  
758 way range from 12.5 to 24.6  $\mu\text{T}$  in the lower reverse-polarity section, the transitional  
759 flow yields 25.2  $\mu\text{T}$  and the upper normal-polarity section provide higher values  
760 between 29.9 and 41.5  $\mu\text{T}$ . All obtained intensity values lie below the present field  
761 strength in Georgia (about 50  $\mu\text{T}$ ). The reverse polarity lower part yielded relatively  
762 low-paleointensity values, characteristic of pre-reversal stages (Laj and Channell,  
763 2007). The relatively high paleointensity values recorded in the upper part of normal  
764 polarity may reflect the intensity recovery after a complete reversal.  
765

766 Comparison of MSP-DB and MSP-DSC results with known field values for the  
767 same location and age shows a paleointensity overestimation by the method without  
768 corrections, also reported in some previous studies (Michalk et al., 2008a, 2010; Fabian  
769 and Leonhardt, 2010; Calvo-Rathert et al., 2016), in contrast to other works where the  
770 results from both protocols are similar or the MSP-DB protocol underestimates the  
771 paleointensity values (Muxworthy and Taylor, 2011; De Groot et al., 2012; Tema et al.,  
772 2015, 2016; Calvo-Rathert et al., 2018). Therefore, according our results, the MSP-DB  
773 method is not independent of domain structure. Moreover, the introduced correction  
774 steps with the MSP-DSC protocol prevent paleointensity overestimation, and thus it is  
775 recommended to use the MSP-DSC protocol instead of the original MSP-DB one.  
776

777 Yet, no generalized agreement may be reached about the quality criteria used in  
778 MSP paleointensity determinations and their threshold values. In the present study we  
779 prefer to use  $\text{CI}_{95}$  (95% confidence interval, see Multispecimen Paleointensity 1.5.  
780 software online version [http://ambre.gm.univ-montp2.fr/camps/MSP\\_DSC](http://ambre.gm.univ-montp2.fr/camps/MSP_DSC)) over  $\Delta B$   
781 ( $\Delta H$  in Fabian and Leonhardt, (2010) as a measure for the final uncertainty of the

782 determination. It should be noted, however that  $CI_{95}$  is calculated through  
783 bootstrapping and is only valid if the bootstrapped values have a Gaussian distribution.  
784 We also propose a less strict threshold (10-15%, depending on determination quality  
785 level) for the relative alteration error  $\epsilon_{alt}$ , than previously recommended by Monster et  
786 al. (2015a and b). In some determinations, in which MSP-DSC paleointensities were  
787 close to those obtained with Thellier-type methods, the f-factor was below the  
788 required 0.2 threshold. This evidences that reliability criteria still need to be analyzed  
789 in detail.

790

## 791 **Acknowledgements**

792

793 This work was supported by project CGL2012-32149 (MINECO, Spain), project  
794 BU066U16 (Junta de Castilla y León, Spain) and pre-doctoral grant BES-2013-064060  
795 (MINECO, Spain). MCR acknowledges funding from the Fulbright Commission and the  
796 Spanish Ministry of Science, Innovation and Universities for a research stay at Hawaii  
797 University at Manoa. AG is grateful to the financial support given by DGAPA-PAPIIT  
798 IN101717. At Montpellier laboratory, the FURemAG rapid furnace construction was  
799 supported by the French National Agency for Research (ANR-12-BS06-0015). Datasets  
800 for this research are available in these in-text data citation references: Sánchez-  
801 Moreno, E. M. (2020). Thellier and multispecimen paleointensities from Apnia Pliocene  
802 volcanic sequence [Data set]. Zenodo. <http://doi.org/10.5281/zenodo.3673186>

803

## 804 **References**

805

- 806 Adamia, S., Zakariadze, G., Chkhotua, T., Sadradze, N., Tsereteli, N., Chabukiani, A.,  
807 Gventsadze, A., 2011. Geology of the Caucasus: A Review. Turkish J. Earth Sci. J.  
808 Earth Sci.) Copyr. ©TÜBİTAK 20, 489–544. <https://doi.org/10.3906/yer-1005-11>
- 809 Avagyan, A., Sosson, M., Karakhanian, A., Philip, H., Rebai, S., Rolland, Y., Melkonyan,  
810 R., Davtyan, V., 2010. Recent tectonic stress evolution in the Lesser Caucasus and  
811 adjacent regions. Geol. Soc. London, Spec. Publ. 340, 393–408.  
812 <https://doi.org/10.1144/sp340.17>
- 813 Besse, J., and V. Courtillot (2002). Apparent and true polar wander and the geometry  
814 of the geomagnetic field over the last 200 Myr, J. Geophys. Res., 107(B11), 2300,  
815 [doi:10.1029/2000JB000050](https://doi.org/10.1029/2000JB000050).
- 816 Biggin, A.J., Paterson, G. a., 2014. A new set of qualitative reliability criteria to aid  
817 inferences on palaeomagnetic dipole moment variations through geological time.  
818 Front. Earth Sci. 2, 1–9. <https://doi.org/10.3389/feart.2014.00024>
- 819 Biggin, A.J., Perrin, M., and Shaw, J., 2007. A comparison of a quasi-perpendicular  
820 method of absolute palaeointensity determination with other thermal and  
821 microwave techniques, 257, 564–581. <https://doi.org/10.1016/j.epsl.2007.03.016>
- 822 Biggin, A.J., Piispa, E.J., Pesonen, L.J., Holme, R., Paterson, G.A., Veikkolainen, T., Tauxe,  
823 L., 2015. Palaeomagnetic field intensity variations suggest Mesoproterozoic inner-  
824 core nucleation. Nature 526, 245–248. <https://doi.org/10.1038/nature15523>
- 825 Biggin, A.J., Poidras, T., 2006. First-order symmetry of weak-field partial  
826 thermoremanence in multi-domain ferromagnetic grains. 1. Experimental

827 evidence and physical implications. *Earth Planet. Sci. Lett.* 245, 438–453.  
828 <https://doi.org/10.1016/j.epsl.2006.02.035>

829 Calvo-Rathert, M., Bógalo, M.F., Gogichaishvili, A., Sologashvili, J., Vashakidze, G.,  
830 2013. New paleomagnetic and paleointensity data from Pliocene lava flows from  
831 the Lesser Caucasus. *J. Asian Earth Sci.* 73, 347–361.  
832 <https://doi.org/10.1016/j.jseaes.2013.04.039>

833 Calvo-Rathert, M., Morales-Contreras, J., Carrancho, Á., Goguitchaichvili, A., 2016. A  
834 comparison of Thellier-type and multispecimen paleointensity determinations on  
835 Pleistocene and historical lava flows from Lanzarote (Canary Islands, Spain).  
836 *Geochemistry, Geophys. Geosystems* 17, 3638–3654.  
837 <https://doi.org/10.1002/2016GC006396>

838 Cromwell, G., Tauxe, L., Staudigel, H., Ron, H., 2015. Paleointensity estimates from  
839 historic and modern Hawaiian lava flows using glassy basalt as a primary source  
840 material. *Phys. Earth Planet. Inter.* 241, 44–56.  
841 <https://doi.org/10.1016/j.pepi.2014.12.007>

842 de Groot, L. V., Béguin, A., Koster, M.E., van Rijsingen, E.M., Struijk, E.L.M., Biggin,  
843 A.J., Hurst, E.A., Langereis, C.G., Dekkers, M.J., 2015. High paleointensities for the  
844 Canary Islands constrain the Levant geomagnetic high. *Earth Planet. Sci. Lett.* 419,  
845 154–167. <https://doi.org/10.1016/j.epsl.2015.03.020>

846 de Groot, L. V., Biggin, A.J., Dekkers, M.J., Langereis, C.G., Herrero-Bervera, E., 2013.  
847 Rapid regional perturbations to the recent global geomagnetic decay revealed by  
848 a new hawaiian record. *Nat. Commun.* 4, 1–7.  
849 <https://doi.org/10.1038/ncomms3727>

850 de Groot, L. V., Dekkers, M.J., Mullender, T.A.T., 2012. Exploring the potential of  
851 acquisition curves of the anhysteretic remanent magnetization as a tool to detect  
852 subtle magnetic alteration induced by heating. *Phys. Earth Planet. Inter.* 194–195,  
853 71–84. <https://doi.org/10.1016/j.pepi.2012.01.006>

854 de Groot, L. V., Dekkers, M. J., Visscher, M., and Ter Maat, G. W., 2014. Magnetic  
855 properties and paleointensities as function of depth in a Hawaiian lava flow.  
856 *Geochemistry, Geophysics, Geosystems*, 15(4), 1096–1112.  
857 <https://doi.org/10.1002/2013GC005094>

858 de Groot, L. V., Pimentel, A., Di Chiara, A., 2016. The multimethod palaeointensity  
859 approach applied to volcanics from Terceira: Full-vector geomagnetic data for the  
860 past 50 kyr. *Geophys. J. Int.* 206, 590–604. <https://doi.org/10.1093/gji/ggw095>

861 Dekkers, M.J., Böhnell, H.N., 2006. Reliable absolute palaeointensities independent of  
862 magnetic domain state. *Earth Planet. Sci. Lett.* 248, 507–516.  
863 <https://doi.org/10.1016/j.epsl.2006.05.040>

864 Dunlop, D.J., 2011. Physical basis of the Thellier–Thellier and related paleointensity  
865 methods. *Phys. Earth Planet. Inter.* 187, 118–138.  
866 <https://doi.org/10.1016/j.pepi.2011.03.006>

867 Dunlop, D. J. and Özdemir, Ö., 2000. Effect of grain size and domain state on thermal  
868 demagnetization tails. *Geophysical Research Letters*, 27(9), 1311–1314.  
869 <https://doi.org/10.1029/1999GL008461>

870 Fabian, K. and Leonhardt, R., 2010. Multiple-specimen absolute paleointensity  
871 determination: An optimal protocol including pTRM normalization, domain-state  
872 correction, and alteration test. *Earth Planet. Sci. Lett.* 297, 84–94.  
873 <https://doi.org/10.1016/j.epsl.2010.06.006>

874 Fabian, K. and Leonhardt, R., 2007. Theoretical analysis and experimental tests of  
875 multiple specimen absolute paleointensity determination techniques, in:  
876 Geophysical Research Abstracts. p. 04510.

877 Fanjat, G., 2012. *Les fluctuations du champ magnétique terrestre : des variations*  
878 *séculaires récentes aux renversements*. PhD. Géosciences, Université de  
879 Montpellier. 768 p. Retrieved from [https://tel.archives-ouvertes.fr/tel-](https://tel.archives-ouvertes.fr/tel-00719380/PDF/theseфанjat2012.pdf)  
880 [00719380/PDF/theseфанjat2012.pdf](https://tel.archives-ouvertes.fr/tel-00719380/PDF/theseфанjat2012.pdf)

881 Haggerty, S.E., 1991. Oxide Textures: A Mini-Atlas, in: Lindsley, D.H. (Ed.), Oxide  
882 Minerals: Petrologic and Magnetic Significance, Rev. Mineral., Vol. 25. Mineral.  
883 Soc. of Am., Washington, D. C., pp. 129–137.

884 Herrero-Bervera, E., Valet, J.-P.P., 1999. Paleosecular variation during sequential  
885 geomagnetic reversals from Hawaii. *Earth Planet. Sci. Lett.* 171, 139–148.  
886 [https://doi.org/10.1016/S0012-821X\(99\)00145-4](https://doi.org/10.1016/S0012-821X(99)00145-4)

887 Kissel, C. and Laj, C., 2004. Improvements in procedure and paleointensity selection  
888 criteria (PICRIT-03) for Thellier and Thellier determinations: Application to  
889 Hawaiian basaltic long cores. *Physics of the Earth and Planetary Interiors*, 147(2–3  
890 SPEC.ISS.), 155–169. <https://doi.org/10.1016/j.pepi.2004.06.010>

891 Laj, C. and Channell, J.E.T., 2007. Geomagnetic Excursions, in: *Treatise on Geophysics*.  
892 Elsevier, pp. 373–416. <https://doi.org/10.1016/B978-044452748-6.00095-X>

893 Lebedev, V.A., 2015. Geological map of Javakheti volcanic area (Lesser Caucasus),  
894 1/200000, (2015). <https://doi.org/10.13140/RG.2.1.6102359.2169>

895 Lebedev, V.A., Bubnov, S.N., Dudaauri, O.Z., Vashakidze, G.T., 2008. Geochronology of  
896 Pliocene volcanism in the Dzhavakheti Highland (the Lesser Caucasus). Part 1:  
897 Western part of the Dzhavakheti Highland. *Stratigr. Geol. Correl.* 16, 204–224.  
898 <https://doi.org/10.1134/S0869593808020081>

899 Leonhardt, R., Heunemann, C., and Krasa, D., 2004. Analyzing absolute paleointensity  
900 determinations: Acceptance criteria and the software ThellierTool4.0.  
901 *Geochemistry, Geophysics, Geosystems*, 5(12), 1–11.  
902 <https://doi.org/10.1029/2004GC000807>

903 Maisuradze, G.M., Kuloshvili, S.I., 1999. “Some Geological Problems of Late Volcanism  
904 in the Dzhavakheti Upland.” *Tr. GIN AN Gruz. Nov. Ser.* 114, 220–228.

905 Michalk, D.M., Biggin, A.J., Knudsen, M.F., Böhnell, H.N., Nowaczyk, N.R., Ownby, S.,  
906 López-Martínez, M., 2010. Application of the multispecimen palaeointensity  
907 method to Pleistocene lava flows from the Trans-Mexican Volcanic Belt. *Phys.*  
908 *Earth Planet. Inter.* 179, 139–156. <https://doi.org/10.1016/j.pepi.2010.01.005>

909 Michalk, D.M., Muxworthy, A.R., Böhnell, H.N., Maclennan, J., Nowaczyk, N., Harald,  
910 N.B., Maclennan, J., Nowaczyk, N., 2008. Evaluation of the multispecimen parallel  
911 differential pTRM method: A test on historical lavas from Iceland and Mexico.  
912 *Geophys. J. Int.* 173, 409–420. <https://doi.org/10.1111/j.1365-246X.2008.03740.x>

913 Monster, M.W.L., de Groot, L. V., Biggin, A.J., Dekkers, M.J., 2015. The performance of  
914 various palaeointensity techniques as a function of rock magnetic behaviour - A  
915 case study for La Palma. *Phys. Earth Planet. Inter.* 242, 36–49.  
916 <https://doi.org/10.1016/j.pepi.2015.03.004>

917 Monster, M.W.L., de Groot, L. V., Dekkers, M.J., 2015. MSP-Tool: A VBA-Based  
918 Software Tool for the Analysis of Multispecimen Paleointensity Data. *Front. Earth*  
919 *Sci.* 3, 1–9. <https://doi.org/10.3389/feart.2015.00086>

920 Monster, M.W.L., Langemeijer, J., Wiarda, L.R., Dekkers, M.J., Biggin, A.J., Hurst, E.A.,

921 Groot, L.V. d., 2018. Full-vector geomagnetic field records from the East Eifel,  
922 Germany. *Phys. Earth Planet. Inter.* 274, 148–157.  
923 <https://doi.org/10.1016/j.pepi.2017.11.009>

924 Muxworthy, A.R., Taylor, S.N., 2011. Evaluation of the domain-state corrected  
925 multiple-specimen absolute palaeointensity protocol: a test of historical lavas  
926 from Iceland. *Geophys. J. Int.* 187, 118–127. <https://doi.org/10.1111/j.1365-246X.2011.05163.x>

928 Paterson, G. A., 2011. A simple test for the presence of multidomain behavior during  
929 paleointensity experiments. *Journal of Geophysical Research: Solid Earth*, 116(10),  
930 1–12. <https://doi.org/10.1029/2011JB008369>

931 Paterson, G.A., Tauxe, L., Biggin, A.J., Shaar, R., Jonestrask, L.C., 2014. On improving  
932 the selection of Thellier-type paleointensity data. *Geochemistry, Geophys.*  
933 *Geosystems* 15, 1180–1192. <https://doi.org/10.1002/2013GC005135>

934 Paterson, G.A., Tauxe, L., Biggin, A.J., Shaar, R., Jonestrask, L.C., 2014. Standard  
935 Paleointensity Definitions v1.1 0–43.

936 Prévot, M., Mankinen, E.A., Coe, R.S., Grommé, C.S., 1985. The Steens Mountain  
937 (Oregon) geomagnetic polarity transition: 2. Field intensity variations and  
938 discussion of reversal models. *J. Geophys. Res. Solid Earth* 90, 10417–10448.  
939 <https://doi.org/10.1029/JB090iB12p10417>

940 Prevot, M., Mankinen, E.A., Gromme, C.S., Coe, R.S., 1985. How the geomagnetic field  
941 vector reverses polarity. *Nature* 316, 230–234. <https://doi.org/10.1038/316230a0>

942 Riisager, J., Perrin, M., Riisager, P., Ruffet, G., 2000. Paleomagnetism, paleointensity  
943 and geochronology of Miocene basalts and baked sediments from Velay Oriental,  
944 French Massif Central. *J. Geophys. Res. Solid Earth* 105, 883–896.  
945 <https://doi.org/10.1029/1999JB900337>

946 Sánchez-Moreno, E.M., 2018. Variation of the absolute paleointensity of the Earth's  
947 magnetic field recorded in sequences of basaltic flows from the volcanic region of  
948 Djavakheti (Georgia). PhD. Universidad de Burgos. 376p.  
949 doi:10.13140/RG.2.2.30939.00804

950 Sánchez-Moreno, E. M., Calvo-Rathert, M., Goguitchaichvili, A., Tauxe, L., Vashakidze,  
951 G. T., Lebedev, V. A. (2020). Weak palaeointensity results over a Pliocene volcanic  
952 sequence from Lesser Caucasus (Georgia): transitional record or time averaged  
953 field? *Geophysical Journal International*, 220(3), 1604–1618.  
954 <https://doi.org/10.1093/gji/ggz533>

955 Sánchez-Moreno, E.M., Calvo-Rathert, M., Goguitchaichvili, A., Vashakidze, G.T.,  
956 Lebedev, V.A., 2018. Evidence of Unusual Geomagnetic Regimes Recorded in Plio-  
957 Pleistocene Volcanic Sequences from the Lesser Caucasus (Southern Georgia).  
958 *Geochemistry, Geophys. Geosystems* 19, 1–18.  
959 <https://doi.org/10.1029/2017GC007358>

960 Sato, M., Yamamoto, Y., Nishioka, T., Kodama, K., Mochizuki, N., Tsunakawa, H., 2016.  
961 Hydrostatic pressure effect on magnetic hysteresis parameters of pseudo-single-  
962 domain magnetite. *Geochemistry, Geophys. Geosystems* 17, 2825–2834.  
963 <https://doi.org/10.1002/2016GC006406>

964 Selkin, P. A., and Tauxe, L., 2000. Long-term variations in palaeointensity. *Philosophical*  
965 *Transactions of the Royal Society A: Mathematical, Physical and Engineering*  
966 *Sciences*, 358(1768), 1065–1088. <https://doi.org/10.1098/rsta.2000.0574>

967 Tauxe, L., 2006. Long-term trends in paleointensity: The contribution of DSDP/ODP

968 submarine basaltic glass collections. *Phys. Earth Planet. Inter.* 156, 223–241.  
969 <https://doi.org/10.1016/j.pepi.2005.03.022>

970 Tauxe, L., Shaar, R., Jonestrask, L., Swanson-Hysell, N.L., Minnett, R., Koppers, A.A.P.,  
971 Constable, C.G., Jarboe, N., Gaastra, K., Fairchild, L., 2016. PmagPy: Software  
972 package for paleomagnetic data analysis and a bridge to the Magnetism  
973 Information Consortium (MagIC) Database. *Geochemistry, Geophys. Geosystems*  
974 17, 2450–2463. <https://doi.org/10.1002/2016GC006307>

975 Tauxe, L., Staudigel, H., 2004. Strength of the geomagnetic field in the Cretaceous  
976 normal superchron: New data from submarine basaltic glass of the Troodos  
977 ophiolite. *Geochemistry, Geophys. Geosystems* 5, 223–241.  
978 <https://doi.org/10.1029/2003GC000635>

979 Tema, E., Camps, P., Ferrara, E., Poidras, T., Nazionale, F.I., Metrologica, R., Tema, E.,  
980 Camps, P., Ferrara, E., Poidras, T., 2015. Directional results and absolute  
981 archaeointensity determination by the classical Thellier and the multi-specimen  
982 DSC protocols for two kilns excavated at Osterietta, Italy. *Stud. Geophys. Geod.*  
983 59, 554–577. <https://doi.org/10.1007/s11200-015-0413-0>

984 Tema, E., Ferrara, E., Camps, P., Conati, C., Spatafora, S., Carvallo, C., Poidras, T., Conati  
985 Barbaro, C., Spatafora, S., Carvallo, C., Poidras, T., 2016. The Earth ' s magnetic  
986 field in Italy during the Neolithic period : New data from the Early Neolithic site of  
987 Portonovo (Marche , Italy). *Earth Planet. Sci. Lett.* 448, 49–61.  
988 <https://doi.org/10.1016/j.epsl.2016.05.003>

989 Thellier, E., Thellier, O., 1959. Sur l'intensité du champ magnétique terrestre dans le  
990 passé historique et géologique. *Ann. Geophys.* 15, 285–376.

991 Yu, Y., Tauxe, L., Genevey, A., 2004. Toward an optimal geomagnetic field intensity  
992 determination technique. *Geochemistry, Geophys. Geosystems* 5, n/a-n/a.  
993 <https://doi.org/10.1029/2003GC000630>

994  
995  
996  
997  
998  
999  
1000  
1001  
1002  
1003  
1004  
1005  
1006  
1007  
1008  
1009  
1010  
1011  
1012  
1013

1014  
 1015  
 1016  
 1017  
 1018  
 1019  
 1020  
 1021  
 1022  
 1023  
 1024  
 1025  
 1026  
 1027

Table 1. *Paleointensity determinations obtained with the multispecimen methods (Biggin and Poidras, 2006; Dekkers and Böhnell, 2006; Fabian and Leonhardt, 2010).*

Site	Spec.	Prot.	N	n	R <sup>2</sup>	f	B ( $\mu$ T)	CI <sub>95</sub> ( $\mu$ T)	CI <sub>95</sub> T/2 ( $\mu$ T)	CI <sub>95</sub> (T/2)% (%)	$\Delta$ B ( $\mu$ T)	$\Delta$ B (%)	$\epsilon_{alt}$ (%)	Class
AP01	03A/04A	DB	8	6	0.9994	-	57.4	[ 56.8 58.0 ]	0.6	1.0				B
		FC	8	7	0.9928	0.33-0.53	55.2	[ 53.2 57.0 ]	1.9	3.4				
		DSC	8	7	0.9814	0.33-0.53	45.1	[ 43.1 47.2 ]	2.1	4.5	7.6	16.9	15.2	B
AP03	04A	DB	8	8	0.9968	-	28.6	[ 27.8 29.4 ]	0.8	2.8				B*
		FC	8	7	0.9981	0.21-0.32	27.7	[ 26.4 28.7 ]	1.2	4.2				
		DSC	8	6	0.9957	0.21-0.32	22.0	[ 21.2 23.1 ]	1.0	4.3	6.7	30.4	15.7	B*
AP04	03BI/All	DB	7	7	0.9859	-	67.1	[ 63.1 70.5 ]	3.7	5.5				B
		FC	4	3	0.9958	0.38-0.46	63.7	[ 58.5 71.5 ]	6.5	10.2				
		DSC	4	4	0.9893	0.38-0.46	55.4	[ 50.7 61.8 ]	5.6	10.0	9.7	17.6	11.0	B
AP05	01B	DB	7	5	0.9406	-	117.5	[ 70.3 158.6 ]	43.9	37.3				-
		FC	4	4	0.8563	0.21-0.32	151.0	[ -670.0 885.6 ]	777.8	515.1				
		DSC	4	3	0.9991	0.21-0.32	100.4	[ 96.9 104.2 ]	3.6	3.5	23.7	23.6	5.4	B
AP10	04A	DB	8	8	0.9935	-	32.4	[ 30.9 33.6 ]	1.4	4.2				B
		FC	8	6	0.9909	0.34-0.44	31.1	[ 27.2 33.9 ]	3.4	10.8				
		DSC	8	6	0.9938	0.30-0.44	25.5	[ 23.5 27.2 ]	1.9	7.3	3.9	15.1	10.7	B
AP11	02A	DB	8	8	0.9687	-	21.9	[ 16.7 27.4 ]	5.4	24.4				-
		FC	8	6	0.9886	0.11-0.19	20.0	[ 17.5 21.9 ]	2.2	11.0				
		DSC	8	6	0.9971	0.11-0.19	15.7	[ 15.1 16.3 ]	0.6	3.8	4.7	30.0	9.5	T <sup>v</sup>
AP12	07BII/CII	DB	7	6	0.7872	-	46.4	[ -258.5 336.0 ]	297.3	640.6				-
		FC	4	3	0.9988	0.24-0.35	49.9	[ 47.7 52.0 ]	2.2	4.3				
		DSC	4	4	0.9830	0.24-0.35	36.8	[ 30.9 41.6 ]	5.4	14.5	6.3	17.2	7.2	A
AP14	06B	DB	7	6	0.9858	-	13.6	[ 10.4 17.3 ]	3.5	25.4				B
		FC	4	4	0.9998	0.47-0.48	14.4	[ 14.1 14.6 ]	0.3	1.7				
		DSC	4	4	0.9992	0.47-0.48	14.0	[ 13.5 14.4 ]	0.5	3.2	0.5	3.7	2.6	A
AP15	07A/BII	DB	7	5	0.4624	-	52.8	[ -12.2 131.3 ]	71.8	135.9				-
		FC	4	3	0.9649	0.10-0.18	27.1	[ 10.5 36.6 ]	13.1	48.2				
		DSC	4	3	0.9493	0.10-0.18	27.2	[ 18.0 34.5 ]	8.3	30.3	0.3	1.2	3.6	T <sup>v</sup>
AP17	06AII/BII	DB	7	6	0.9825	-	26.6	[ 24.8 28.2 ]	1.7	6.4				B
		FC	5	3	0.9953	0.24-0.33	28.1	[ 25.6 30.9 ]	2.7	9.4				
		DSC	5	3	0.9965	0.24-0.33	22.6	[ 21.0 24.2 ]	1.6	7.1	5.9	26.2	8.4	B

AP19	01BII/CII	DB	7	6	0.9946	-	26.2	[ 25.3 27.0 ]	0.9	3.2				-
		FC	5	4	0.9931	0.07-0.14	24.2	[ 20.8 26.7 ]	3.0	12.2				
		DSC	5	5	0.9784	0.07-0.14	19.2	[ 16.3 21.8 ]	2.8	14.3	3.7	19.4	3.4	T <sup>v</sup>
AP20	07B/09C	DB	8	7	0.9381	-	4.1	[ -10.9 23.5 ]	17.2	423.6				-
		FC	8	4	0.9914	0.26-0.32	14.6	[ 13.4 16.3 ]	1.5	9.9				
		DSC	8	4	0.9593	0.26-0.32	11.0	[ 9.05 13.7 ]	2.3	21.1	5.6	51.1	35.4	T <sup>v</sup>

1028 *Note.* Site: Lava flow name. Spec.: Specimen sub-name. Prot.: MSP type protocol. N:  
1029 Number specimens with different B<sub>lab</sub> applied in the experiment. n: Number specimens  
1030 with different B<sub>lab</sub> used in the determination. Experimental statistics: R<sup>2</sup>, f, Cl<sub>95</sub> T/2, Cl<sub>95</sub>  
1031 (T/2)% , ΔB and ε<sub>alt</sub> (Table S2). B: Paleointensity. Class: Determination quality level. Tv:  
1032 Determinations that have not passed selection criteria, but their agreement with  
1033 Thellier-type results has driven us to consider them for final paleointensity  
1034 calculations.

1035 Table 2. *Paleointensity averaged for each lava flow and for each the absolute paleointensity determination method.*

Site	TT				IZZI				MSP-DB			MSP-FC			MSP-DSC					
	n	B (μT)	σB (μT)	σB (%)	n	B (μT)	σB (μT)	σB (%)	n	B (μT)	95% CI (μT)	95% CI <sub>T/2</sub> (%)	n	B (μT)	95% CI (μT)	95% CI <sub>T/2</sub> (%)	n	B (μT)	95% CI (μT)	95% CI <sub>T/2</sub> (%)
AP01	2	17.8	1.8	10.4	1	37.8	0.8	2.0	6	57.4	[56.8 - 58.0]	1.0	7	55.2	[53.2 - 57.0]	3.4	7	45.1	[43.1 - 47.2]	4.5
AP02	2	41.0	3.5	8.7	4	35.1	2.1	6.1												
AP04	3	33.5	8.4	25.0	4	34.1	1.7	5.1	7	67.1	[63.1 - 70.5]	5.5	3	63.7	[58.5 - 71.5]	10.2	4	55.4	[50.7 - 61.8]	10.0
AP05					4	29.9	7.3	19.5	5	117.5	[70.3 - 158.6]	37.3	4	151.0	[-670.0 - 885.6]	515.1	3	100.4	[96.9 - 104.2]	3.5
AP03	1	39.6	2.4	6.0					8	28.6	[27.8 - 29.4]	2.8	7	27.7	[26.4 - 28.7]	4.2	6	22.0	[21.2 - 23.1]	4.3
AP06					3	25.2	1.6	6.5												
AP07	1	12.9	0.5	4.0	2	19.6	0.5	2.6												
AP08	1	23.6	1.1	4.5																
AP09	3	16.6	0.7	4.4																
AP10	2	12.9	0.6	4.5					8	32.4	[30.9 - 33.6]	4.2	6	31.1	[27.2 - 33.9]	10.8	6	25.5	[23.5 - 27.2]	7.3
AP12	2	13.6	0.4	2.6					6	46.4	[-258.5 - 336.0]	640.6	3	49.9	[47.7 - 52.0]	4.3	4	36.8	[30.9 - 41.6]	14.5
AP11	2	20.3	3.1	15.5	4	24.9	4.6	18.3	8	21.9	[16.7 - 27.4]	24.4	6	20.0	[17.5 - 21.9]	11.0	6	15.7	[15.1 - 16.3]	3.8
AP13	1	13.0	0.7	5.0	2	12.2	0.2	1.4												
AP14	3	19.6	1.3	6.8	6	20.3	0.7	3.4	6	13.6	[10.4 - 17.3]	25.4	4	14.4	[14.1 - 14.6]	1.7	4	14.0	[13.5 - 14.4]	3.2
AP15	1	23.9	1.6	6.9					5	52.8	[-12.2 - 131.3]	135.9	3	27.1	[10.5 - 36.6]	48.2	3	27.2	[18.0 - 34.5]	30.3
AP16					5	16.8	2.3	13.9												
AP17	2	20.2	4.0	19.6	7	26.1	4.7	21.9	6	26.6	[24.8 - 28.2]	6.4	3	28.1	[25.6 - 30.9]	9.4	3	22.6	[21.0 - 24.2]	7.1
AP18	1	24.7	0.5	2.0	4	23.1	1.1	4.6												
AP20	2	16.4	1.9	11.8	3	16.8	0.8	4.7	7	4.1	[-10.9 - 23.5]	423.6	4	14.6	[13.4 - 16.3]	9.9	4	11.0	[9.1 - 13.7]	21.1
AP19	2	20.9	0.8	4.1	5	21.3	1.0	1.9	6	26.2	[25.3 - 27.0]	3.2	4	24.2	[20.8 - 26.7]	12.2	5	19.2	[16.3 - 21.8]	14.3

1036 *Note.* All the paleointensities obtained by the multispecimen method are shown, although the quality criteria are not fulfilled.

Table 3. Final weighted average paleointensities per lava flow in the Apnia sequence.

age (Ma)	Site	Q	MSP			Weighted average					
			TT	IZZI	DSC	B ( $\mu$ T)	sd ( $\mu$ T)	sd (%)	VADM ( $10^{22}$ Am <sup>2</sup> )	$\sigma$ VADM ( $10^{22}$ Am <sup>2</sup> )	
3.09	AP01	1	+	1	1	41.5	5.2		12.5	7.1	0.88
3.09	AP02	2	2	4	-	37.1	3.0		8.2	6.3	0.52
3.09	AP04	2	3	4	+	33.8	0.3		0.9	5.8	0.05
3.09	AP05	3	x	4	+	29.9	7.3	sd*	24.4	5.1	1.24
3.28	AP03	4	1	x	+	39.6	2.4	$\sigma$ PI	6.0	6.7	0.40
3.28	AP06	3	x	3	-	25.2	1.6	sd*	6.3	4.3	0.27
3.75	AP07	2	1	2	-	17.4	3.9		22.3	3.0	0.66
3.75	AP08	4	1	x	-	23.6	1.1	$\sigma$ PI	4.5	4.0	0.18
3.75	AP09	3	3	x	-	16.6	0.7	sd*	4.2	2.8	0.12
3.75	AP10	4	2	x	+	12.9	0.6	sd*	4.7	2.2	0.10
3.70	AP12	4	2	x	+	13.6	0.4	sd*	2.9	2.3	0.07
3.70	AP11	2	2	4	x	23.4 (22.3)	2.4 (3.6)		10.2 (16.3)	4.0 (3.8)	0.40 (0.61)
3.70	AP13	2	1	2	-	12.5	0.5		3.7	2.1	0.08
3.70	AP14	1	3	6	1	19.4	2.1		10.7	3.3	0.35
3.70	AP15	2	1	x	x	23.9 (25.6)	1.6 (2.3)	$\sigma$ PI	6.9 (9.1)	4.1 (4.4)	0.28 (0.39)
3.70	AP16	3	x	5	-	16.8	2.3	sd*	13.7	2.9	0.39
3.70	AP17	1	2	7	1	24.6	2.5		10.4	4.2	0.43
3.70	AP18	2	1	4	-	23.4	0.7		3.1	4.0	0.12
3.70	AP20	2	3	3	x	16.6 (16.0)	0.2 (2.0)		1.3	2.8 (2.7)	0.04 (0.34)
3.70	AP19	2	2	5	x	21.2 (20.9)	0.2 (0.7)		0.9 (3.5)	3.6 (3.6)	0.03 (0.12)

+ rejected by paleointensity value

x rejected by quality criteria

- not measured

 $\sigma$ B  $\pm$  single paleointensity determination error calculated from the Arai plot linear regression

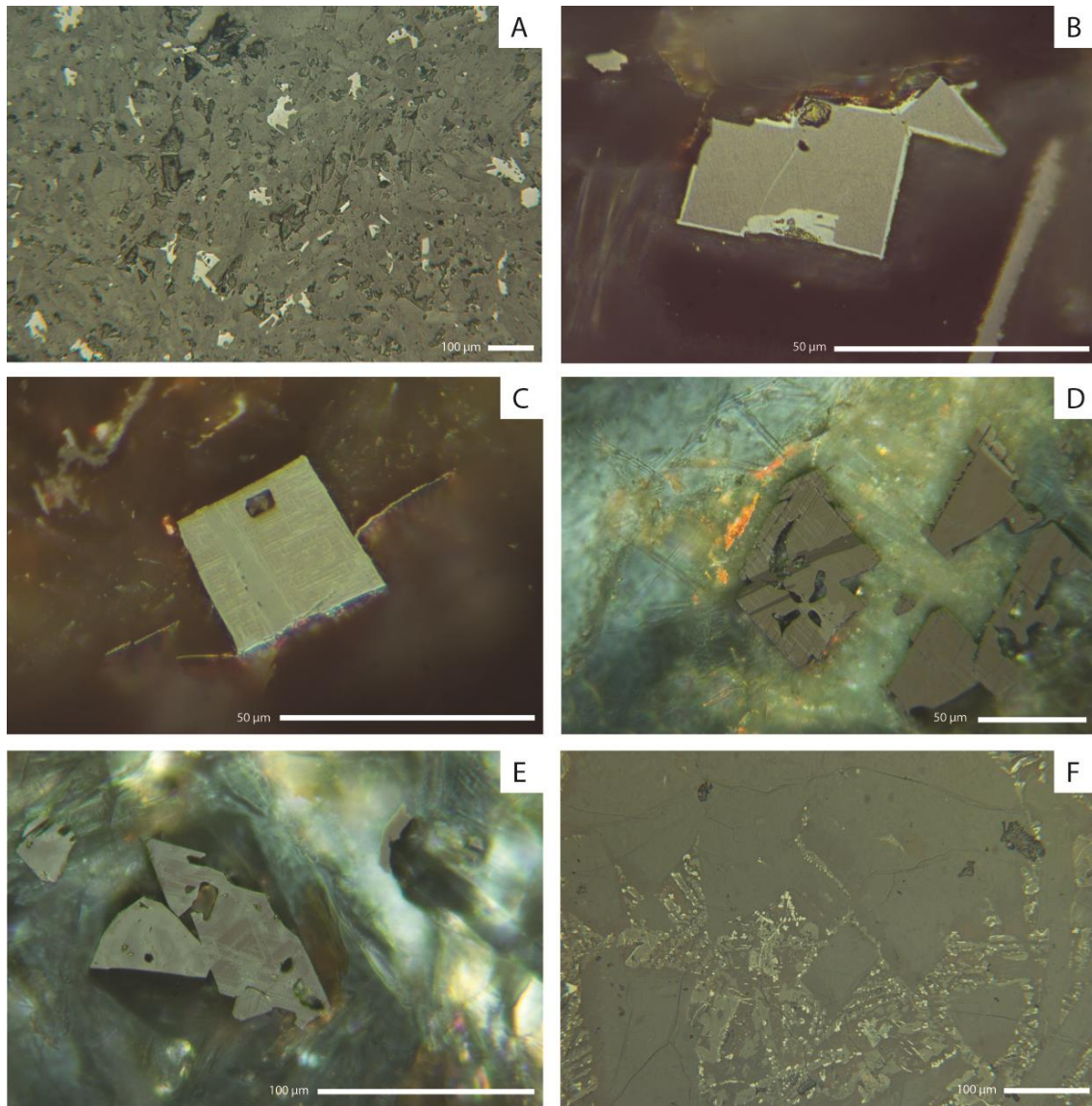
sd\* standard deviation of the paleointensities obtained from a single lava flow

( ) averaged paleointensity calculated with MSP-DSC of bad quality match with Thellier results

1038 *Note.* Final weighted paleointensity average calculated by lava flow using the number  
1039 of individual determinations (note that in the case of multispecimen determinations,  
1040 although several specimens are used for a single determination the weighted value  
1041 remains equal to 1). The number of determinations performed with each method is  
1042 shown. Those methods rejected by paleointensity value, or quality criteria or those not  
1043 measured are indicated. Q: quality paleointensity average level. TT: Thellier-Thellier  
1044 (1959); IZZI: In-field/Zero-field protocol (Yu et al., 2004); MSP-DSC: Multispecimen  
1045 domain-state correction (Fabian and Leonhardt, 2010); *sd* ( $\mu$ T and %): standard  
1046 deviation by lava flow (see table for especial cases). VADM: Virtual axial dipole  
1047 moment.  $\sigma$ VADM: Virtual axial dipole moment error calculated from *sd* ( $\mu$ T).

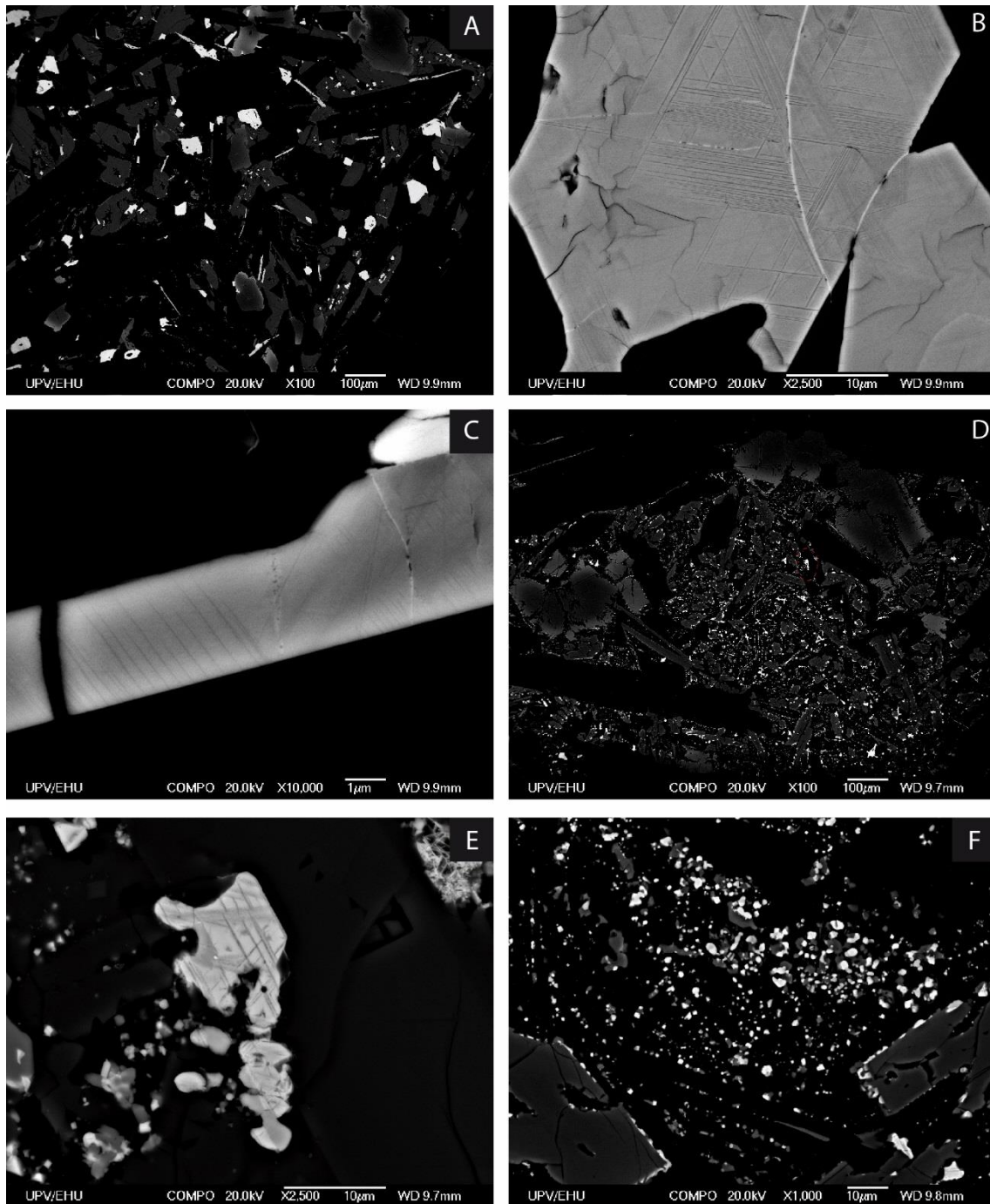
1048

1049



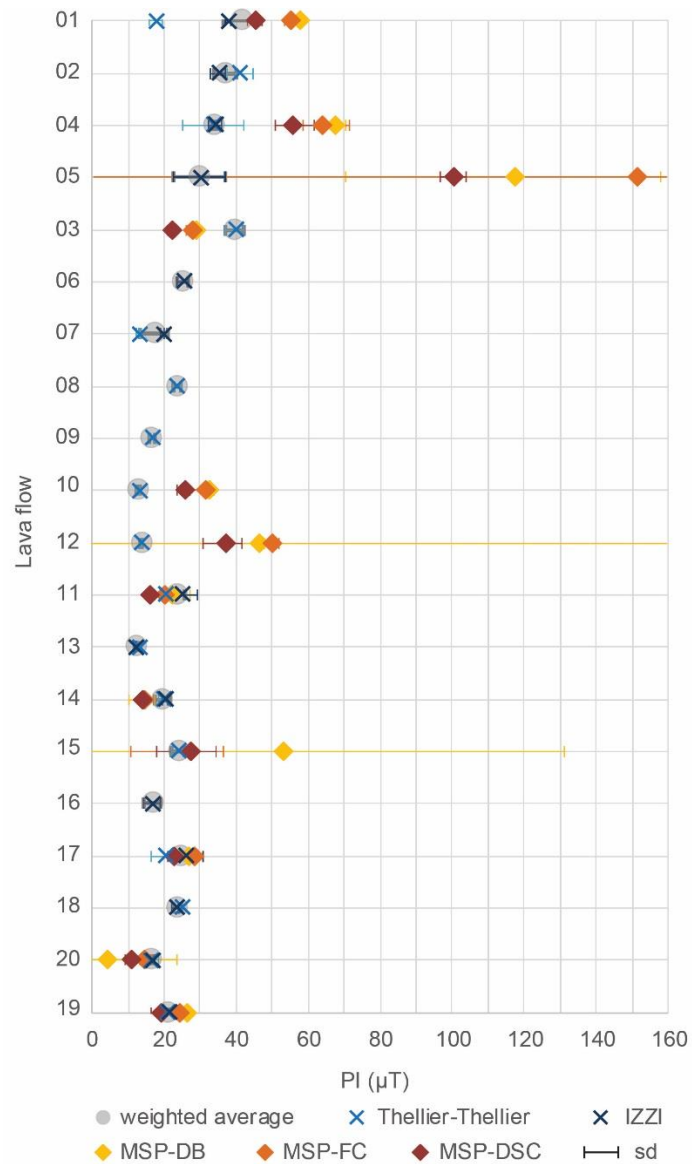
1050  
 1051  
 1052  
 1053  
 1054  
 1055  
 1056  
 1057  
 1058  
 1059

Figure 1. Reflected light optical microscope images of polished thin sections from the Apnia sequence. (a) Overview image of the AP02 sample showing the distribution of euhedral to subhedral crystals. (b) Detailed image of a titanite crystal from AP06 with maghemitization on the crystal edges. (c) and (d) Euhedral titanomagnetite crystal from AP13 with Trellis and Sandwich intergrowths of ilmenite, indicative of C3 oxidation stage. (e) Titanomagnetite crystal with Trellis ilmenite intergrowths pointing out a C3 oxidation stage (AP06). (f) Detailed view of micron-sized titanomagnetite crystals disseminated in AP14.



1060  
 1061  
 1062  
 1063  
 1064  
 1065  
 1066  
 1067  
 1068  
 1069  
 1070  
 1071

Figure 2. Scanning electron microscope (SEM) images of polished thin sections from the Apnia sequence. (a) Overview image of the AP06 sample showing the distribution of euhedral to subhedral crystals. (b) Detailed image of a titanite crystal from AP06 with Trellis intergrowths of ilmenite, indicative of C3 oxidation stage, and micro-cracks around the crystal boundaries due to maghemitization. (c) Detail of an acicular ilmenite crystal showing exsolved rutile needles, evidence of R2 oxidation stage. Sample AP06. (d) General view of the sample AP08 showing the small size and skeletal morphologies of the opaque minerals. The dash-red circle indicates the crystal of image (e). (e) Titanomagnetite crystal with Trellis and Sandwich ilmenite intergrowths pointing out a C3 oxidation stage (AP08). (f) Detailed view of micron-sized titanomagnetite crystals disseminated in AP08.



1072  
 1073  
 1074  
 1075  
 1076  
 1077  
 1078

Figure 3. Final weighted average paleointensities per lava flow in the Apnia sequence. TT: Thellier-Thellier (1959); IZZI: In-field Zero-field protocol (Yu et al., 2004); MSP-DB: Multispecimen parallel differential pTRM method (Biggin and Poidras, 2006; Dekkers and Böhnelt, 2006); MSP-FC: Multispecimen with fraction correction (Fabian and Leonhardt, 2010); MSP-DSC: Multispecimen with domain-state correction (Fabian and Leonhardt, 2010); sd: standard deviation.

Site	Spec.	Prot.	N	n	R <sup>2</sup>	f	B (μT)	Cl <sub>95</sub> (μT)	Cl <sub>95</sub> T/2 (μT)	Cl <sub>95</sub> (T/2)% (%)	ΔB (μT)	ΔB (%)	ε <sub>alt</sub> (%)	Class
AP01	03A/04A	DB	8	6	0.9994	-	57.4	[ 56.8 58.0 ]	0.6	1.0				B
		FC	8	7	0.9928	0.33-0.53	55.2	[ 53.2 57.0 ]	1.9	3.4				
		DSC	8	7	0.9814	0.33-0.53	45.1	[ 43.1 47.2 ]	2.1	4.5	7.6	16.9	15.2	B
AP03	04A	DB	8	8	0.9968	-	28.6	[ 27.8 29.4 ]	0.8	2.8				B*
		FC	8	7	0.9981	0.21-0.32	27.7	[ 26.4 28.7 ]	1.2	4.2				
		DSC	8	6	0.9957	0.21-0.32	22.0	[ 21.2 23.1 ]	1.0	4.3	6.7	30.4	15.7	B*
AP04	03BI/All	DB	7	7	0.9859	-	67.1	[ 63.1 70.5 ]	3.7	5.5				B
		FC	4	3	0.9958	0.38-0.46	63.7	[ 58.5 71.5 ]	6.5	10.2				
		DSC	4	4	0.9893	0.38-0.46	55.4	[ 50.7 61.8 ]	5.6	10.0	9.7	17.6	11.0	B
AP05	01B	DB	7	5	0.9406	-	117.5	[ 70.3 158.6 ]	43.9	37.3				-
		FC	4	4	0.8563	0.21-0.32	151.0	[ -670.0 885.6 ]	777.8	515.1				
		DSC	4	3	0.9991	0.21-0.32	100.4	[ 96.9 104.2 ]	3.6	3.5	23.7	23.6	5.4	B
AP10	04A	DB	8	8	0.9935	-	32.4	[ 30.9 33.6 ]	1.4	4.2				B
		FC	8	6	0.9909	0.34-0.44	31.1	[ 27.2 33.9 ]	3.4	10.8				
		DSC	8	6	0.9938	0.30-0.44	25.5	[ 23.5 27.2 ]	1.9	7.3	3.9	15.1	10.7	B
AP11	02A	DB	8	8	0.9687	-	21.9	[ 16.7 27.4 ]	5.4	24.4				-
		FC	8	6	0.9886	0.11-0.19	20.0	[ 17.5 21.9 ]	2.2	11.0				
		DSC	8	6	0.9971	0.11-0.19	15.7	[ 15.1 16.3 ]	0.6	3.8	4.7	30.0	9.5	T <sup>v</sup>
AP12	07BII/CII	DB	7	6	0.7872	-	46.4	[ -258.5 336.0 ]	297.3	640.6				-
		FC	4	3	0.9988	0.24-0.35	49.9	[ 47.7 52.0 ]	2.2	4.3				
		DSC	4	4	0.9830	0.24-0.35	36.8	[ 30.9 41.6 ]	5.4	14.5	6.3	17.2	7.2	A
AP14	06B	DB	7	6	0.9858	-	13.6	[ 10.4 17.3 ]	3.5	25.4				B
		FC	4	4	0.9998	0.47-0.48	14.4	[ 14.1 14.6 ]	0.3	1.7				
		DSC	4	4	0.9992	0.47-0.48	14.0	[ 13.5 14.4 ]	0.5	3.2	0.5	3.7	2.6	A
AP15	07A/BII	DB	7	5	0.4624	-	52.8	[ -12.2 131.3 ]	71.8	135.9				-
		FC	4	3	0.9649	0.10-0.18	27.1	[ 10.5 36.6 ]	13.1	48.2				
		DSC	4	3	0.9493	0.10-0.18	27.2	[ 18.0 34.5 ]	8.3	30.3	0.3	1.2	3.6	T <sup>v</sup>
AP17	06AII/BII	DB	7	6	0.9825	-	26.6	[ 24.8 28.2 ]	1.7	6.4				B
		FC	5	3	0.9953	0.24-0.33	28.1	[ 25.6 30.9 ]	2.7	9.4				
		DSC	5	3	0.9965	0.24-0.33	22.6	[ 21.0 24.2 ]	1.6	7.1	5.9	26.2	8.4	B
AP19	01BII/CII	DB	7	6	0.9946	-	26.2	[ 25.3 27.0 ]	0.9	3.2				-
		FC	5	4	0.9931	0.07-0.14	24.2	[ 20.8 26.7 ]	3.0	12.2				
		DSC	5	5	0.9784	0.07-0.14	19.2	[ 16.3 21.8 ]	2.8	14.3	3.7	19.4	3.4	T <sup>v</sup>
AP20	07B/09C	DB	8	7	0.9381	-	4.1	[ -10.9 23.5 ]	17.2	423.6				-
		FC	8	4	0.9914	0.26-0.32	14.6	[ 13.4 16.3 ]	1.5	9.9				
		DSC	8	4	0.9593	0.26-0.32	11.0	[ 9.05 13.7 ]	2.3	21.1	5.6	51.1	35.4	T <sup>v</sup>

Site	TT			IZZI			MSP-DB			MSP-FC					
	n	B ( $\mu$ T)	$\sigma$ B ( $\mu$ T)	$\sigma$ B (%)	n	B ( $\mu$ T)	$\sigma$ B ( $\mu$ T)	$\sigma$ B (%)	n	B ( $\mu$ T)	95% CI ( $\mu$ T)	95% CI <sub>T/2</sub> (%)	n	B ( $\mu$ T)	95% CI ( $\mu$ T)
AP01	2	17.8	1.8	10.4	1	37.8	0.8	2.0	6	57.4	[56.8 - 58.0]	1.0	7	55.2	[53.2 - 57.0]
AP02	2	41.0	3.5	8.7	4	35.1	2.1	6.1							
AP04	3	33.5	8.4	25.0	4	34.1	1.7	5.1	7	67.1	[63.1 - 70.5]	5.5	3	63.7	[58.5 - 71.5]
AP05					4	29.9	7.3	19.5	5	117.5	[70.3 - 158.6]	37.3	4	151.0	[-670.0 - 885.6]
AP03	1	39.6	2.4	6.0					8	28.6	[27.8 - 29.4]	2.8	7	27.7	[26.4 - 28.7]
AP06					3	25.2	1.6	6.5							
AP07	1	12.9	0.5	4.0	2	19.6	0.5	2.6							
AP08	1	23.6	1.1	4.5											
AP09	3	16.6	0.7	4.4											
AP10	2	12.9	0.6	4.5					8	32.4	[30.9 - 33.6]	4.2	6	31.1	[27.2 - 33.9]
AP12	2	13.6	0.4	2.6					6	46.4	[-258.5 - 336.0]	640.6	3	49.9	[47.7 - 52.0]
AP11	2	20.3	3.1	15.5	4	24.9	4.6	18.3	8	21.9	[16.7 - 27.4]	24.4	6	20.0	[17.5 - 21.9]
AP13	1	13.0	0.7	5.0	2	12.2	0.2	1.4							
AP14	3	19.6	1.3	6.8	6	20.3	0.7	3.4	6	13.6	[10.4 - 17.3]	25.4	4	14.4	[14.1 - 14.6]
AP15	1	23.9	1.6	6.9					5	52.8	[-12.2 - 131.3]	135.9	3	27.1	[10.5 - 36.6]
AP16					5	16.8	2.3	13.9							
AP17	2	20.2	4.0	19.6	7	26.1	4.7	21.9	6	26.6	[24.8 - 28.2]	6.4	3	28.1	[25.6 - 30.9]
AP18	1	24.7	0.5	2.0	4	23.1	1.1	4.6							
AP20	2	16.4	1.9	11.8	3	16.8	0.8	4.7	7	4.1	[-10.9 - 23.5]	423.6	4	14.6	[13.4 - 16.3]
AP19	2	20.9	0.8	4.1	5	21.3	1.0	1.9	6	26.2	[25.3 - 27.0]	3.2	4	24.2	[20.8 - 26.7]

95% CI <sub>T/2</sub> (%)	n	B (μT)	MSP-DSC	
			95% CI (μT)	95% CI <sub>T/2</sub> (%)
3.4	7	45.1	[43.1 - 47.2]	4.5
10.2	4	55.4	[50.7 - 61.8]	10.0
515.1	3	100.4	[96.9 - 104.2]	3.5
4.2	6	22.0	[21.2 - 23.1]	4.3
10.8	6	25.5	[23.5 - 27.2]	7.3
4.3	4	36.8	[30.9 - 41.6]	14.5
11.0	6	15.7	[15.1 - 16.3]	3.8
1.7	4	14.0	[13.5 - 14.4]	3.2
48.2	3	27.2	[18.0 - 34.5]	30.3
9.4	3	22.6	[21.0 - 24.2]	7.1
9.9	4	11.0	[9.1 - 13.7]	21.1
12.2	5	19.2	[16.3 - 21.8]	14.3

age (Ma)	Site	Q	MSP			Weighted average			VADM	$\sigma$ VADM
			TT	IZZI	DSC	B ( $\mu$ T)	sd ( $\mu$ T)	sd (%)	( $10^{22}$ Am <sup>2</sup> )	( $10^{22}$ Am <sup>2</sup> )
3.09	AP01	1	+	1	1	41.5	5.2	12.5	7.1	0.88
3.09	AP02	2		2	4	37.1	3.0	8.2	6.3	0.52
3.09	AP04	2		3	4	33.8	0.3	0.9	5.8	0.05
3.09	AP05	3	x	4	+	29.9	7.3	sd* 24.4	5.1	1.24
3.28	AP03	4	1	x	+	39.6	2.4	$\sigma$ PI 6.0	6.7	0.40
3.28	AP06	3	x	3	-	25.2	1.6	sd* 6.3	4.3	0.27
3.75	AP07	2	1	2	-	17.4	3.9	22.3	3.0	0.66
3.75	AP08	4	1	x	-	23.6	1.1	$\sigma$ PI 4.5	4.0	0.18
3.75	AP09	3	3	x	-	16.6	0.7	sd* 4.2	2.8	0.12
3.75	AP10	4	2	x	+	12.9	0.6	sd* 4.7	2.2	0.10
3.70	AP12	4	2	x	+	13.6	0.4	sd* 2.9	2.3	0.07
3.70	AP11	2	2	4	x	23.4 (22.3)	2.4 (3.6)	10.2 (16.3)	4.0 (3.8)	0.40 (0.61)
3.70	AP13	2	1	2	-	12.5	0.5	3.7	2.1	0.08
3.70	AP14	1	3	6	1	19.4	2.1	10.7	3.3	0.35
3.70	AP15	2	1	x	x	23.9 (25.6)	1.6 (2.3)	$\sigma$ PI 6.9 (9.1)	4.1 (4.4)	0.28 (0.39)
3.70	AP16	3	x	5	-	16.8	2.3	sd* 13.7	2.9	0.39
3.70	AP17	1	2	7	1	24.6	2.5	10.4	4.2	0.43
3.70	AP18	2	1	4	-	23.4	0.7	3.1	4.0	0.12
3.70	AP20	2	3	3	x	16.6 (16.0)	0.2 (2.0)	1.3	2.8 (2.7)	0.04 (0.34)
3.70	AP19	2	2	5	x	21.2 (20.9)	0.2 (0.7)	0.9 (3.5)	3.6 (3.6)	0.03 (0.12)

+ rejected by paleointensity value

x rejected by quality criteria

- not measured

$\sigma$ B  $\pm$  single paleointensity determination error calculated from the Arai plot linear regression

sd\* standard deviation of the paleointensities obtained from a single lava flow

( ) averaged paleointensity calculated with MSP-DSC of bad quality match with Thellier results

Figure 1.

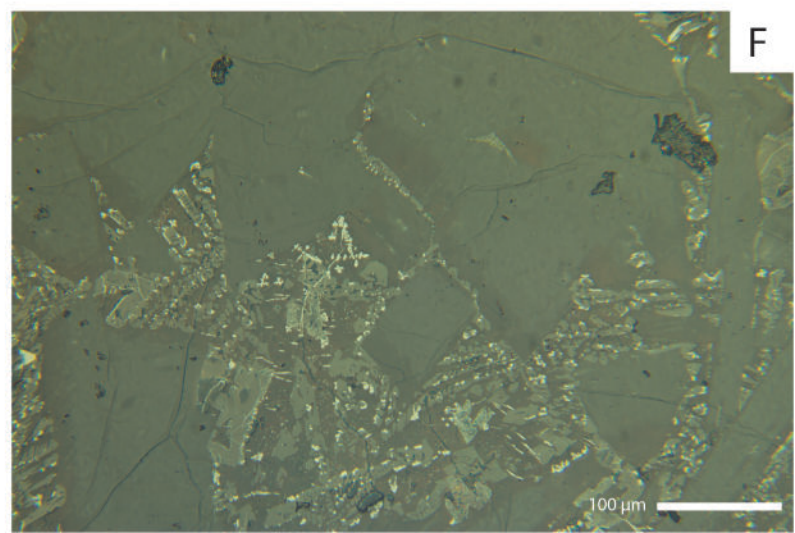
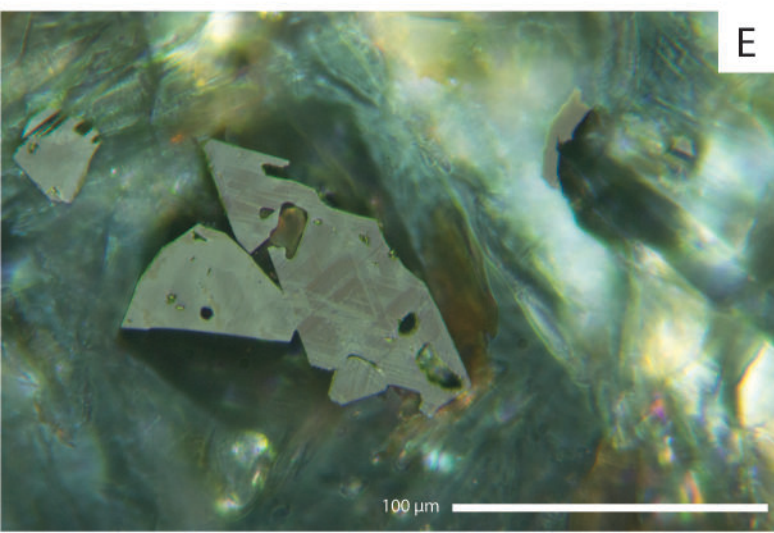
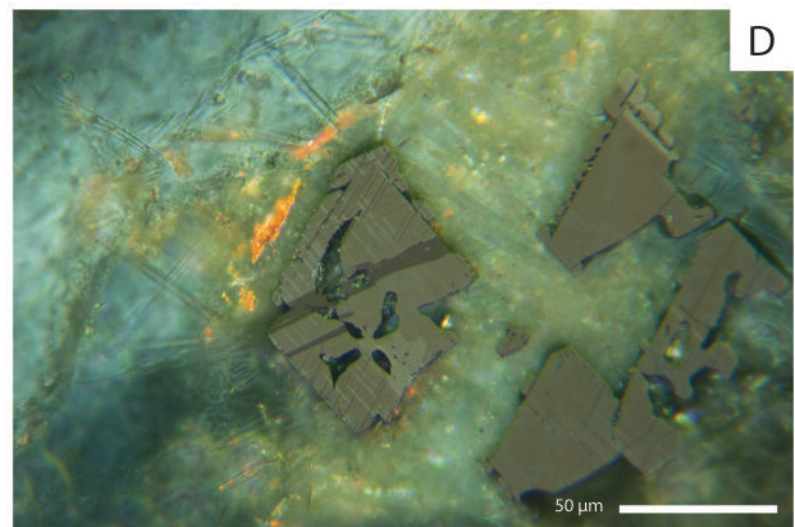
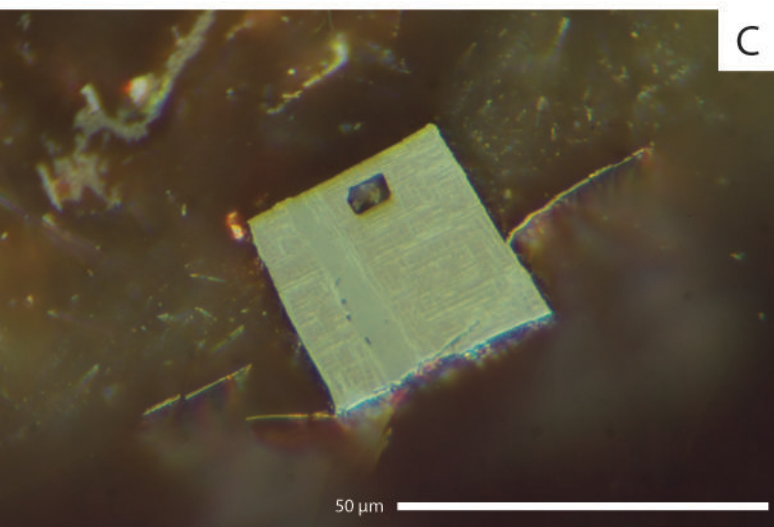
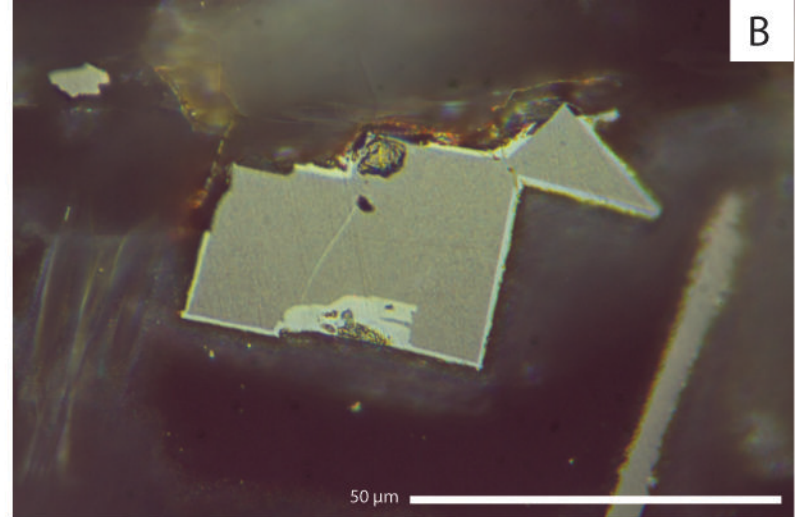
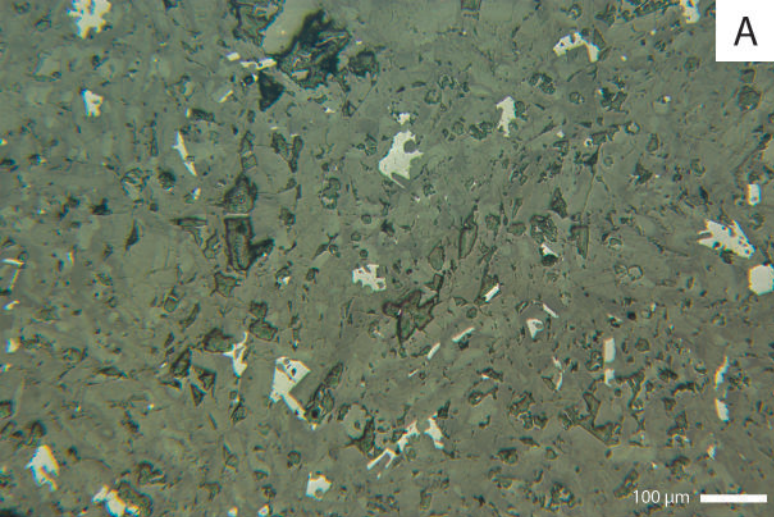


Figure 2.

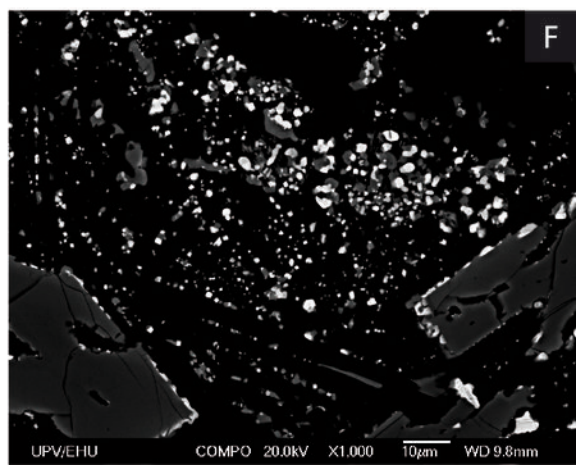
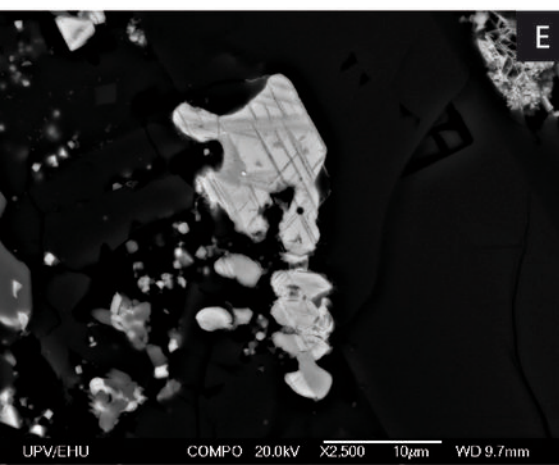
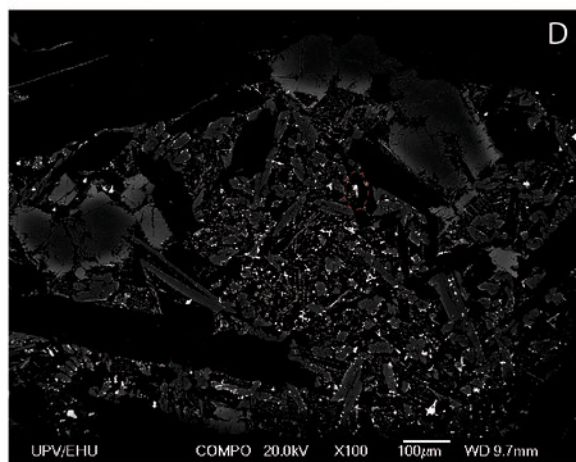
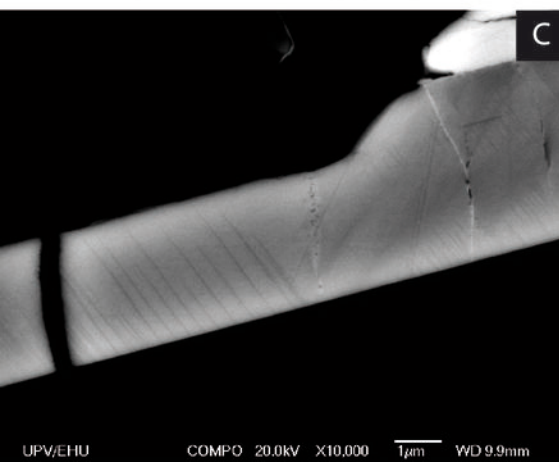
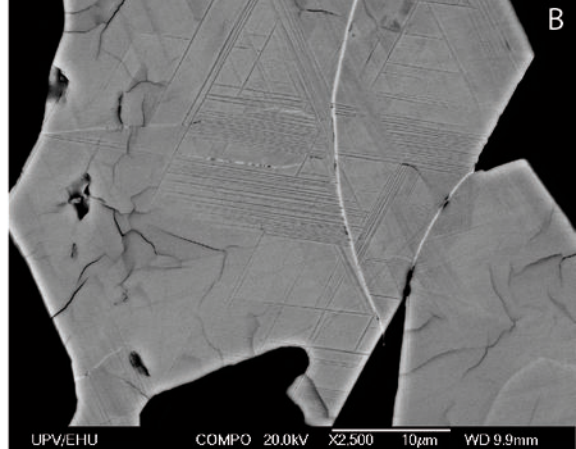
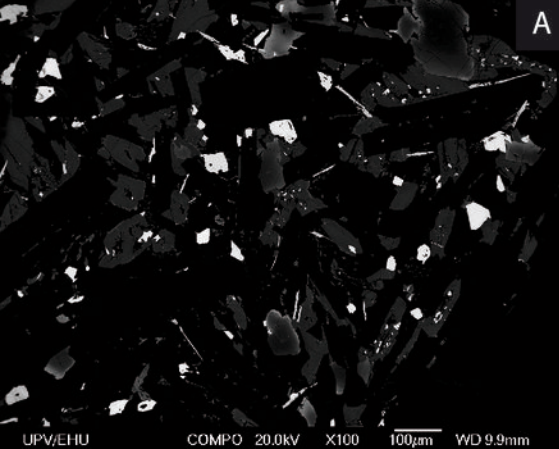


Figure 3.

